

# Sequence Domain SISO Equivalent Models of a Grid-Tied Voltage Source Converter System for Small-Signal Stability Analysis

Chen Zhang, Xu Cai, Atle Rygg, and Marta Molinas, *Member, IEEE*

**Abstract**—This paper presents a generalized method for converting multi-input and multi-output (MIMO)  $dq$  impedance model of a grid-tied voltage source converter system into its sequence domain single-input and single-output (SISO) equivalents. As a result, two types of SISO impedance models were derived, one of which was derived from relatively strong and  $dq$  symmetric grid assumption (reduced SISO model) and the other was based on closed-loop equivalent (accurate SISO model). It was proven that the accurate SISO model has the same marginal stability condition as the MIMO model. Accuracy of these models is assessed with respect to the measured impedances in PSCAD/EMTDC simulations, their effects on stability are analyzed as well. Findings show that the accurate SISO model presents identical stability conclusions as the MIMO model. However, the reduced SISO model may lead to inaccurate results if the system is highly  $dq$  asymmetric, e.g., VSC with fast phase-locked loop or an actively controlled grid.

**Index Terms**—Couplings, PLL, sequence impedance, stability analysis, voltage source converter.

## I. INTRODUCTION

NOWADAYS, voltage source converters (VSC) have become widely used in grid-integrated renewable energies [1] and flexible power transmission systems [2]. Oscillations at both low [3] and high frequencies [4] were observed in VSC-based systems, particularly in weak grid conditions [5]. Such types of small-signal stability issues can be effectively assessed by impedance-based analysis. Impedance models of three-phase VSCs [6]–[9], single-phase VSCs [10], and modular multi-level converters [11], among others, have been developed rigorously in recent literature.

For typical two-level and three-phase grid-tied VSCs, the impedance can be extracted either in  $dq$  synchronously rotating frame [7] or in three-phase stationary frame [8]. In  $dq$

Manuscript received April 24, 2017; revised July 9, 2017 and September 5, 2017; accepted October 18, 2017. This work was supported by grants from the Power Electronics Science and Education Development Program of the Delta Environmental and Educational Foundation (DREM2016005). Paper no. TEC-00310-2017. (*Corresponding author: Chen Zhang.*)

C. Zhang and X. Cai are with the Department of Electrical Engineering, Shanghai Jiao Tong University, Shanghai 200240, China (e-mail: nealbc@sjtu.edu.cn; xucai@sjtu.edu.cn).

A. Rygg and M. Molinas are with the Department of Engineering Cybernetics, Norwegian University of Science and Technology, Trondheim 7491, Norway (e-mail: atle.rygg@ntnu.no; marta.molinas@ntnu.no).

Color versions of one or more of the figures in this paper are available online at <http://ieeexplore.ieee.org>.

Digital Object Identifier 10.1109/TEC.2017.2766217

frame, the grid-tied VSC system is time invariant if grid is three-phase balanced. This setup allows for direct linearization; thus, performing Laplace transformation on the resultant linear time invariant (LTI) model yields  $dq$  impedances [9]. However, if applied to three-phase stationary frame, the grid-tied VSC inherently varies by time. Therefore, the harmonic linearization method from a previous study [12] is applied to obtain sequence impedances [8]. Generally, linearizing the time-varying system along a steady periodic trajectory yields a linear time periodic (LTP) system. To transform LTP systems into frequency domain, the harmonic balance approach [13] can be adopted.

Despite the different models in  $dq$  and sequence domains, both are coupled because of the off-diagonal terms in impedance matrices are nonzero. Recent research has presented interest in the interpretation of these couplings and their consequences during stability assessment. Previous works [14], [15] established that frequency couplings can be identified in their sequence domain (i.e., positive and negative sequences are coupled and separated by twice fundamental frequency); and their impacts on low-frequency stability were also emphasized. This interesting property of VSC was also identified from  $dq$  impedance and introduced as  $dq$  asymmetry in [16]. Moreover, the relationship between  $dq$  and sequence impedances were thoroughly investigated in [17], and findings showed that  $dq$  impedances can be transformed into its modified sequence domain equivalents by means of symmetrical decomposition [18]. On the other hand, a complex space vector method [16] is used to directly derive VSC impedance in stationary frame [19].

However, frequency couplings in the foregoing reviews (e.g., [14]–[17]) were in single-frequency coupling form (i.e., a single-frequency perturbation induces a single-frequency coupling that separated by twice the fundamental frequency). This condition is true if either the converter or the grid impedance is  $dq$  asymmetric [16] or equivalently contains the mirror frequency coupling effect [17]. If the system is three-phase unbalanced, there will be multiple frequency couplings. To include these couplings with full accuracy, the harmonic-state space [20] as well as the harmonic transfer function method [13] should be adopted.

Currently, both cases on single- and multiple-frequency couplings can only be captured by matrix-based impedances, which are multi-input and multi-output (MIMO) systems by nature; therefore, the generalized Nyquist criterion (GNC) [21] should be adopted for stability analysis. Furthermore, finding the

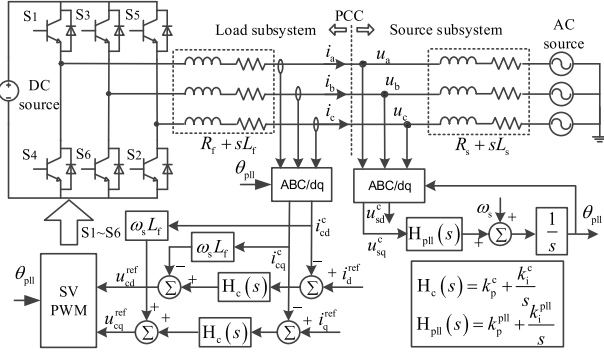


Fig. 1. Schematic of the grid-tied VSC system.

single-input and single-output (SISO) equivalents of grid-tied VSC system is appealing due to their simplicity and convenience for physical interpretation.

This paper aims to develop a generalized method for converting MIMO dq impedance into its sequence domain SISO equivalents by exploring the properties of single-frequency coupling system. The rest of the paper is organized as follows: In Section II, the method for converting the dq impedance into its MIMO sequence domain equivalents is introduced. System blocks of a grid-tied VSC system are modeled based on this method. In Section III, sequence domain MIMO model of grid-tied VSC system is established by assembling the blocks in Section II. And its SISO equivalents are found by performing closed-loop analysis of the entire system, instead of viewing them as subsystems. A detailed comparison of SISO models with measured impedances in PSCAD/EMTDC is presented. Section IV discussed the performance of proposed SISO models in predicting small signal stability. Finally, Section V draws the conclusions.

## II. MODELING OF GRID-TIED VSC IN MODIFIED SEQUENCE DOMAIN

### A. Topology and Control Scheme of the Grid-Tied VSC

Fig. 1 presents the system analyzed in this paper. It constitutes a typical two-level VSC, an L-type filter, and a Thevenin-equivalent grid.

Only current controller and phase-locked loop (PLL) are considered, mainly to achieve simplicity of subsequent property analysis. It will not affect the generality of proposed method as will be presented later. Grid voltage feedforwards can have a great impacts on both transient [6] and small-signal response [5] of VSC, if the bandwidths of these feedforwards are not carefully chosen. In this regard, feedforwards are viewed as impedance-shaping method, and will not be discussed in this paper because the focus is on modeling.

### B. Symmetrical Decomposition of a dq Impedance

Taking a dq impedance model in [9] as an example,

$$\begin{bmatrix} U_d(s) \\ U_q(s) \end{bmatrix} = \begin{bmatrix} Z^{dd}(s) & Z^{dq}(s) \\ Z^{qd}(s) & Z^{qq}(s) \end{bmatrix} \begin{bmatrix} I_d(s) \\ I_q(s) \end{bmatrix} \quad (1)$$

Expression (1) is a LTI system and a complex exponential input (e.g.,  $e^{st}$ ) leads to an output with the same formation. Thus, the variables for dq currents and voltages in (1) can be written explicitly with variable  $s$ , as shown below.

$$\begin{bmatrix} U_d \\ U_q \end{bmatrix} e^{st} = \begin{bmatrix} Z^{dd}(s) & Z^{dq}(s) \\ Z^{qd}(s) & Z^{qq}(s) \end{bmatrix} \begin{bmatrix} I_d \\ I_q \end{bmatrix} e^{st}, \forall s \rightarrow j\omega \quad (2)$$

where  $s \rightarrow j\omega$  is translated from  $s$ -domain to frequency-domain.  $I_d, I_q$  and  $U_d, U_q$  are the current and voltage phasors at frequency  $\omega$  respectively, and they can be decomposed as:

$$\begin{bmatrix} U_p \\ U_n \end{bmatrix} = \frac{1}{2} \begin{bmatrix} 1 & j \\ 1 & -j \end{bmatrix} \begin{bmatrix} U_d \\ U_q \end{bmatrix} = \mathbf{A} \begin{bmatrix} U_d \\ U_q \end{bmatrix} \quad (3)$$

Applying matrix  $\mathbf{A}$  and its inverse  $\mathbf{A}^{-1}$  to (2) yields:

$$\begin{bmatrix} U_p \\ U_n \end{bmatrix} = \mathbf{A} \begin{bmatrix} Z^{dd}(s) & Z^{dq}(s) \\ Z^{qd}(s) & Z^{qq}(s) \end{bmatrix} \mathbf{A}^{-1} \begin{bmatrix} I_p \\ I_n \end{bmatrix} = \mathbf{Z}^{PN}(s) \begin{bmatrix} I_p \\ I_n \end{bmatrix}, \forall s \rightarrow j\omega \quad (4)$$

where elements in  $\mathbf{Z}^{PN}(s) = \begin{bmatrix} Z^{dd}(s) & Z^{dq}(s) \\ Z^{qd}(s) & Z^{qq}(s) \end{bmatrix}$  are generally complex transfer functions. This method makes it possible to obtain the modified sequence impedance directly from well-developed dq impedance as discussed in [17] (i.e., the same authors of this paper). The term ‘‘modified’’ denotes the specific frequency notation used in [17], where the frequency of sequence impedances is referred to dq frame. This notation is adopted in the present paper as well, and the term ‘‘modified’’ will be omitted for brevity in subsequent analysis. However, other recent works e.g., [14] and [19] use a different frequency notation, which are referred to phase domain.

### C. Sequence Domain System Blocks of Grid-Tied VSC

Adopting the decomposition method in Section II-B, system blocks of a grid-tied VSC system in dq format (e.g., [9]) can be transformed into their sequence domain equivalents.

For passive circuit elements, e.g., filter:

$$\begin{bmatrix} R_f + sL_f & -\omega_s L_f \\ \omega_s L_f & R_f + sL_f \end{bmatrix} \xrightarrow{\text{dq-pn}} \begin{bmatrix} Z_f^{pp}(s) & 0 \\ 0 & Z_f^{nn}(s) \end{bmatrix} \quad (5)$$

where  $Z_f^{pp}(s) = R_f + sL_f + j\omega_s L_f$ ,  $Z_f^{nn}(s) = \bar{Z}_f^{pp}(s)$ . The upper line on the latter denotes complex-conjugate operator on the function (i.e., the coefficients not the Laplace variable ‘‘s’’). For a typical Thevenin grid, its sequence impedances are similarly as the filter, which are  $Z_s^{pp}(s) = R_s + sL_s + j\omega_s L_s$  and  $Z_s^{nn}(s) = \bar{Z}_s^{pp}(s)$  respectively.

For variables perturbed by abc to dq transformation e.g., converter output currents:

$$\begin{bmatrix} 0 & \frac{I_{c0} T_{pll}(s)}{U_0} \\ 0 & -\frac{I_{cd0} T_{pll}(s)}{U_0} \end{bmatrix} \xrightarrow{\text{dq-pn}} \frac{T_{pll}(s)}{2U_0} \begin{bmatrix} -I_{c0} & I_{c0} \\ I_{c0}^* & -I_{c0}^* \end{bmatrix} \quad (6)$$

where  $T_{pll}(s) = \frac{U_0 H_{pll}(s)}{s + U_0 H_{pll}(s)}$  is the closed-loop system of a typical PLL as in Fig. 1.  $U_0$  is the voltage at PLL sampling point.

151  $\underline{I}_{c0} = I_{cd0} + jI_{cq0}$  is the complex-valued current in steady.  
 152 The converter output voltage can be obtained similarly as:  
 153  $\frac{T_{pll}(s)}{2U_0} \begin{bmatrix} -\underline{U}_{c0} & \underline{U}_{c0} \\ \underline{U}_{c0} & -\underline{U}_{c0}^* \end{bmatrix} \cdot \underline{U}_{c0} = U_{cd0} + jU_{cq0}$  is the complex-valued  
 154 converter terminal voltage.

155 For current controller it has:

$$\begin{bmatrix} H_c(s) & 0 \\ 0 & H_c(s) \end{bmatrix} \xrightarrow{\text{dq-pn}} \begin{bmatrix} H_c^{pp}(s) & 0 \\ 0 & H_c^{nn}(s) \end{bmatrix} \quad (7)$$

156 Generally, all the system blocks in dq domain can be trans-  
 157 formed into their sequence domain equivalents, e.g., VSC with  
 158 PQ controller, DC voltage controller etc.

#### 159 D. Sequence Impedance Model of the Grid-Tied VSC System

160 The sequence domain MIMO model of a grid-tied VSC sys-  
 161 tem can be established by assembling system blocks derived in  
 162 Section II-C.

163 For a load (VSC) subsystem, its admittance is:

$$-\begin{bmatrix} \mathbf{i}_L^p \\ \mathbf{i}_L^n \end{bmatrix} = \begin{bmatrix} \mathbf{Y}_L^{pp}(s) & \mathbf{Y}_L^{pn}(s) \\ \mathbf{Y}_L^{np}(s) & \mathbf{Y}_L^{nn}(s) \end{bmatrix} \begin{bmatrix} \mathbf{u}_L^p \\ \mathbf{u}_L^n \end{bmatrix} = \mathbf{Y}_L^{PN}(s) \begin{bmatrix} \mathbf{u}_L^p \\ \mathbf{u}_L^n \end{bmatrix} \quad (8)$$

164 For a generalized source (grid) subsystem, its impedance is:

$$\begin{bmatrix} \mathbf{u}_S^p \\ \mathbf{u}_S^n \end{bmatrix} = \begin{bmatrix} \mathbf{Z}_S^{pp}(s) & \mathbf{Z}_S^{pn}(s) \\ \mathbf{Z}_S^{np}(s) & \mathbf{Z}_S^{nn}(s) \end{bmatrix} \begin{bmatrix} \mathbf{i}_S^p \\ \mathbf{i}_S^n \end{bmatrix} = \mathbf{Z}_S^{PN}(s) \begin{bmatrix} \mathbf{i}_S^p \\ \mathbf{i}_S^n \end{bmatrix} \quad (9)$$

$$\mathbf{i}_S^p = \mathbf{i}_L^p, \mathbf{i}_S^n = \mathbf{i}_L^n \quad (10)$$

$$\mathbf{u}_S^p + \mathbf{u}_{ptb}^p = \mathbf{u}_L^p, \mathbf{u}_L^n = \mathbf{u}_S^n \quad (11)$$

165 where  $\mathbf{Y}_L^{pp} = \frac{1-G_{pll}}{H_c^{pp} + Z_f^{pp}}$ ,  $\mathbf{Y}_L^{nn} = \bar{\mathbf{Y}}_L^{pp}$ ,  $\mathbf{Y}_L^{pn} = \frac{G_{pll}}{H_c^{pp} + Z_f^{pp}}$ ,  $\mathbf{Y}_L^{np} =$   
 166  $\bar{\mathbf{Y}}_L^{pn}$  and  $G_{pll} = \frac{T_{pll}(s)}{2U_0} (H_c I_{c0} + \underline{U}_{c0})$ . Laplace variable  $s$  is omit-  
 167 ted for brevity.

168  $\mathbf{u}_{ptb}^p$  is a positive sequence perturbation voltage. Functions in  
 169 bold format e.g.,  $\mathbf{Z}_S^{PN}$  denotes a matrix, in the case of Fig. 1, it  
 170 has  $\mathbf{Z}_S^{pn}(s) = \mathbf{Z}_S^{np}(s) = 0$ , as the grid is passive and dq sym-  
 171 metric. The subscript ‘S’ in capital format denotes source (e.g.,  
 172 grid) subsystem, and ‘L’ denotes load (e.g., VSC) subsystem.  
 173 Note that the line on the letter e.g.,  $\bar{\mathbf{Y}}_L^{pp}$  is conjugate operator on  
 174 the function, if the full complex conjugate operator “\*” is used,  
 175 it has  $(\mathbf{Y}_L^{pp})^* = \bar{\mathbf{Y}}_L^{pp}(\bar{s})$ . The derived MIMO model as (8) and  
 176 (9) can be used directly to assess small-signal stability with the  
 177 help of GNC [14]. A previous study [17] proved that the GNC  
 178 based on this model leads to identical results, as the GNC based  
 179 on dq impedance.

180 The sequence equivalent circuits can be plotted as Fig. 2 on  
 181 the basis of (8)–(11). In Fig. 2, positive and negative sequence  
 182 circuits are coupled via two dependent current sources, which  
 183 are voltage controlled. This intrinsic binding between positive  
 184 and negative sequence circuits will be explored further in next  
 185 section for finding their SISO equivalents.

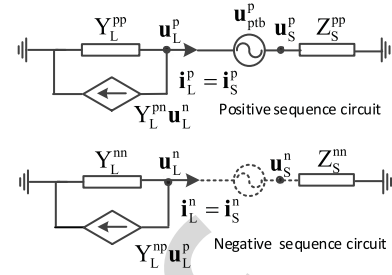


Fig. 2. Sequence domain equivalent circuits of the grid-tied VSC system.

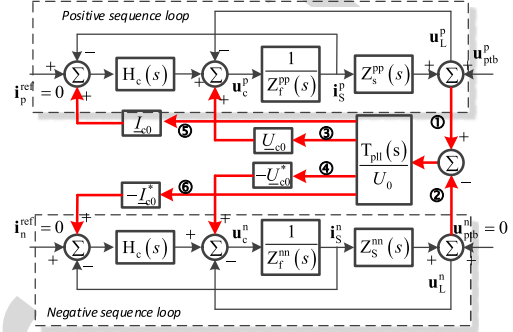


Fig. 3. Sequence domain control blocks diagram of a grid-tied VSC system.

### III. SISO EQUIVALENT MODELS OF A GRID-TIED VSC SYSTEM

#### A. Analysis of Coupled Sequence Loops

In order to reveal the sequence coupling in a more intuitive way, manipulating the system blocks (5)–(7) with electrical system configuration in Fig. 1 yields the following diagram.

Fig. 3 clearly identifies the positive and negative sequence loops coupled via six paths, which are all caused by the PLL (i.e.,  $T_{pll}(s)$ ). Different paths will result in models with different accuracies, as in the following cases:

*Case 1:* By neglecting all paths, the simplest model with decoupled positive and negative sequences is obtained. Although this case may not be effective for stability analysis, it is useful for identifying the intrinsic properties of the grid-VSC system (e.g., resonant point), and the coupling effects of PLL can be introduced as additional damping sources to the intrinsic resonant point [22].

*Case 2:* By isolating the paths of ①③⑤ and ②④⑥, another popular decoupled sequence model as in [8] is obtained. The positive and negative loop impedance from perturbation voltage to the current response can be calculated directly from Fig. 3; i.e.,  $1/\mathbf{Y}_L^{pp} + \mathbf{Z}_S^{pp}$  and  $1/\mathbf{Y}_L^{nn} + \mathbf{Z}_S^{nn}$ . Note that the obtained loop impedance is equivalent to neglect the off-diagonal terms in the converter admittance. This condition is satisfied if the grid is relatively strong and dq symmetric. See the proof in the subsequent analysis as in (18), (19).

The foregoing analysis presents two decoupled models for the grid-tied VSC, which are SISO systems. However, both models neglect sequence coupling to some extent. In the following section, we will develop a method for deriving an accurate SISO model with no assumptions and reductions.



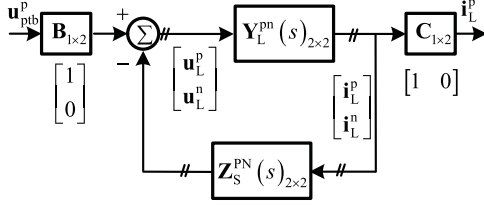


Fig. 4. Closed-loop representation of a grid-tied VSC system.

### B. Accurate and Reduced SISO Models of the Grid-Tied VSC

In this subsection, we regard VSC and grid as a closed-loop system, not as subsystems, perturbed by independent sources. Due to linearity, closed-loop analysis under positive and negative independent perturbations can be analyzed separately.

Taking the positive sequence as an example, the positive sequence loop impedance can be obtained by solving the linear system in Fig. 4:

$$Z_{L_{loop}}^P(s) = -\frac{\mathbf{u}_{ptb}^p}{\mathbf{i}_L^p} = \frac{1}{\mathbf{C}(\mathbf{Z}_L^{PN}(s) + \mathbf{Z}_S^{PN}(s))^{-1}\mathbf{B}} \quad (12)$$

where  $\mathbf{Z}_L^{PN}(s) = (\mathbf{Y}_L^{PN}(s))^{-1}$ . It should be noted that the derived loop impedance is one dimension, i.e., a SISO system.

Substituting elements as in (8) and (9) into (12) yields:

$$Z_{L_{loop}}^P(s) = Z_S^{pp} + Z_L^{pp} - \frac{(Z_L^{np} + Z_S^{np})(Z_L^{pn} + Z_S^{pn})}{Z_S^{nn} + Z_L^{nn}} \quad (13)$$

This method is applied to find the negative sequence loop impedance. Replacing the matrix  $\mathbf{B} = [0 \ 1]^T$ ,  $\mathbf{C} = [0 \ 1]$  and  $\mathbf{u}_{ptb}^p \rightarrow \mathbf{u}_{ptb}^n$  yields:

$$Z_{L_{loop}}^N(s) = Z_S^{nn} + Z_L^{nn} - \frac{(Z_L^{np} + Z_S^{np})(Z_L^{pn} + Z_S^{pn})}{Z_S^{pp} + Z_L^{pp}} \quad (14)$$

Expressions (13) and (14) is defined as the *accurate SISO model*, and  $Z_{L_{loop}}^P(s) = \bar{Z}_{L_{loop}}^N(s)$  still holds, i.e., if we have the analytical model of the positive sequence, the negative sequence model is determined accordingly. In addition, during the derivation, no assumption for dq symmetry was made, therefore this method is general for any LTI systems.

The physical interpretation of this method is: the negative sequence circuit in Fig. 2 is augmented into the positive sequence network (and vice versa) via the voltage-controlled dependent current source. Consequently, the effects of sequence coupling are included in this model intrinsically.

In order to proof the validity of the method, a previous work in [17], where the sequence impedance is derived for source and load subsystem is compared. Taking the positive sequence model for example, in [17] it has:

$$Z_L^p = -\frac{\mathbf{u}_L^p}{\mathbf{i}_L^p} = Z_L^{pp} - \frac{Z_L^{pn}(Z_L^{np} + Z_S^{np})}{Z_S^{nn} + Z_L^{nn}} \quad (15)$$

$$Z_S^p = \frac{\mathbf{u}_S^p}{\mathbf{i}_S^p} = Z_S^{pp} - \frac{Z_S^{pn}(Z_L^{np} + Z_S^{np})}{Z_S^{nn} + Z_L^{nn}} \quad (16)$$

$$Z_L^n(s) = \bar{Z}_L^p(s)$$

$$Z_S^n(s) = \bar{Z}_S^p(s) \quad (17)$$

We can clearly observe that  $Z_L^p + Z_S^p = Z_{L_{loop}}^p$  and  $Z_L^n + Z_S^n = Z_{L_{loop}}^n$ . ((15) and (16) are equivalent to (33) in [17], but are written in a more compact form with slightly different notation.)

Furthermore, if considering a dq symmetric and relatively strong grid, it has conditions as:  $Z_S^{pp} = Z_S^{nn} = 0, |Z_S^{pp}| \ll |Z_L^{pp}|, \forall \omega$  and  $|Z_S^{nn}| \ll |Z_L^{nn}|, \forall \omega$ . Hence, (13) and (14) can be reduced to:

$$Z_{L_{loop}}^{P,rd}u(s) = Z_S^{pp} + \frac{\det |Z_L^{PN}|}{Z_L^{nn}} = Z_S^{pp} + \frac{1}{Y_L^{pp}} \quad (18)$$

$$Z_{L_{loop}}^{N,rd}u(s) = Z_S^{nn} + \frac{\det |Z_L^{PN}|}{Z_L^{pp}} = Z_S^{nn} + \frac{1}{Y_L^{nn}} \quad (19)$$

Expressions (18) and (19) is defined as the *reduced SISO model*, which is widely applied in previous research [8]. However, a frequency translation to phase domain is needed since this paper uses a dq frequency notation.

### C. Proof of Identical Marginal Stability Condition

This subsection will prove that the accurate SISO model is consistent with the MIMO model in terms of marginal stability condition. The marginal stability condition is defined as the case when the eigenvalue loci of a MIMO or SISO system cross the  $(-1, 0)$  point on the basis of GNC or NC.

For MIMO-based model, the marginal stability condition is:

$$\text{There is } s \text{ that eig}(\mathbf{Z}_S^{PN} \cdot \mathbf{Y}_L^{PN}) \text{ equals } -1 + 0 \cdot j \quad (20)$$

where  $\mathbf{Z}_S^{PN}, \mathbf{Y}_L^{PN}$  are given in (8) and (9). After some calculations, we have the equality as:

$$\det \mathbf{Z}_S^{PN} + \det \mathbf{Z}_L^{PN} + Z_S^{pp} Z_L^{nn} + Z_S^{nn} Z_L^{pp} - Z_L^{np} Z_S^{pn} - Z_L^{pn} Z_S^{np} = 0 \quad (21)$$

For SISO-based model, the marginal stability condition is:

$$\text{There is } s \text{ that eig}(Z_S^p/Z_L^p) \text{ equals } -1 + 0 \cdot j \quad (22)$$

where  $Z_S^p, Z_L^p$  are given in (15) and (16).

(22) is equivalent to  $\det |Z_{L_{loop}}^p| = 0 \rightarrow Z_{L_{loop}}^p = 0$ , thus the equality given by (13) is:

$$(Z_S^{nn} + Z_L^{nn})(Z_S^{pp} + Z_L^{pp}) - (Z_L^{pn} + Z_S^{pn})(Z_L^{np} + Z_S^{np}) = 0 \quad (23)$$

Expanding (23), then substitute  $\det \mathbf{Z}_S^{PN} = Z_S^{pp} Z_S^{nn} - Z_S^{pn} Z_S^{np}$  and  $\det \mathbf{Z}_L^{PN} = Z_L^{pp} Z_L^{nn} - Z_L^{pn} Z_L^{np}$  into (23) can prove that (21) equals (23), i.e., the accurate SISO model has the same marginal stability condition as the MIMO model. Therefore it can be used with accuracy in stability analysis. Furthermore, any modifications on SISO model will lead to a marginal stability condition different from (23) e.g., the reduced SISO model. Note that the same proof applies to the negative sequence.

### D. Comparison of SISO Models with Measurements

The accurate SISO model as in (13) and (14), and the reduced SISO model as in (18) and (19), will be compared under conditions of a) dq symmetric and b) dq asymmetric grid.

Impedance measurements conducted in PSCAD/EMTDC with the system in Fig. 1 (see Appendix A for detailed

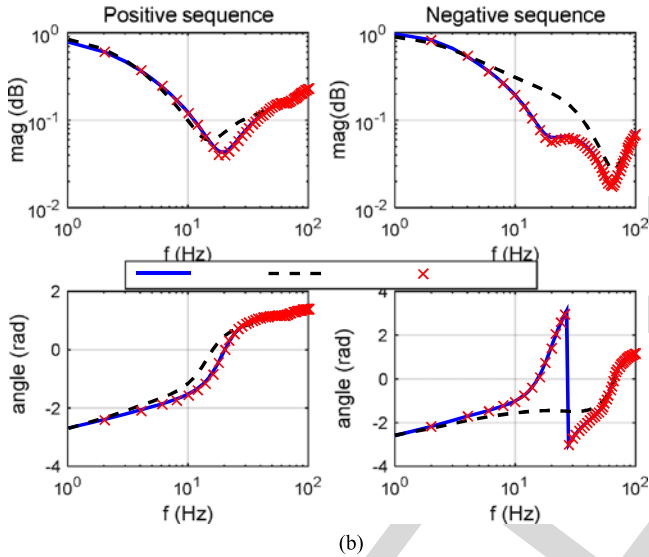
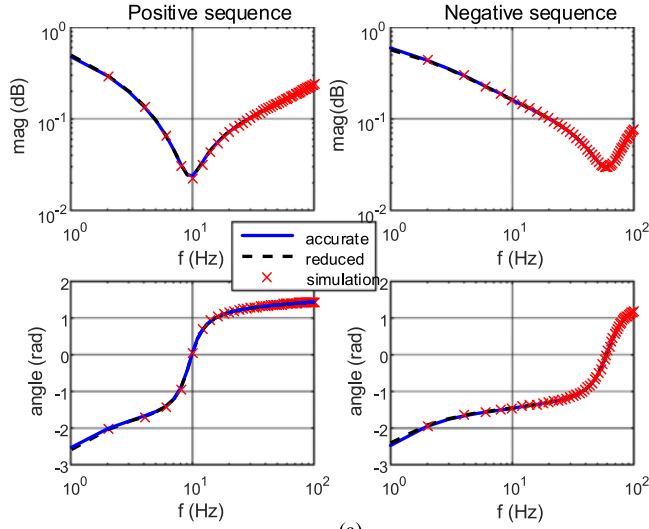


Fig. 5. Loop impedance comparison under dq symmetric grid. (a) SCR = 4, CC = 200 Hz, PLL = 5 Hz, current is 0.5 p.u. (flow out). (b) SCR = 4, CC = 200 Hz, PLL = 200 Hz, current is 0.5 p.u. (flow out).

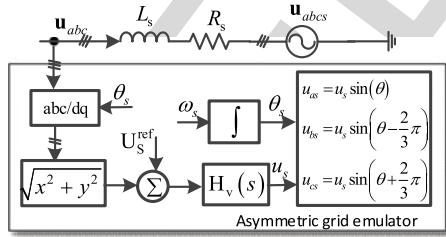


Fig. 6. Control scheme for asymmetric grid emulation.

284 system parameters). The multi-run module in PSCAD is used.  
 285 At each run, a single-tone harmonic voltage is injected into the  
 286 grid. The frequency is varied from 0 Hz to 100 Hz with an increment  
 287 of 2 Hz. The sampling frequency and sampling window  
 288 used for Fourier analysis are 1 kHz and 0.5 s respectively. All  
 289 data and figures are post-processed in MATLAB.

290 1) dq Symmetric Grid Cases: As shown in Fig. 5(a), both  
 291 accurate and reduced SISO models achieved a good match with

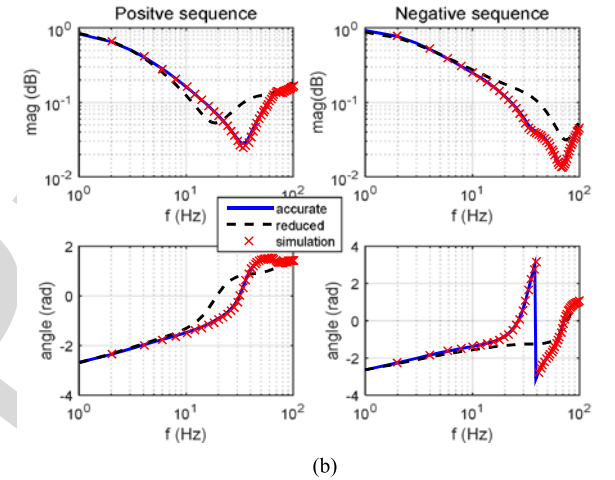
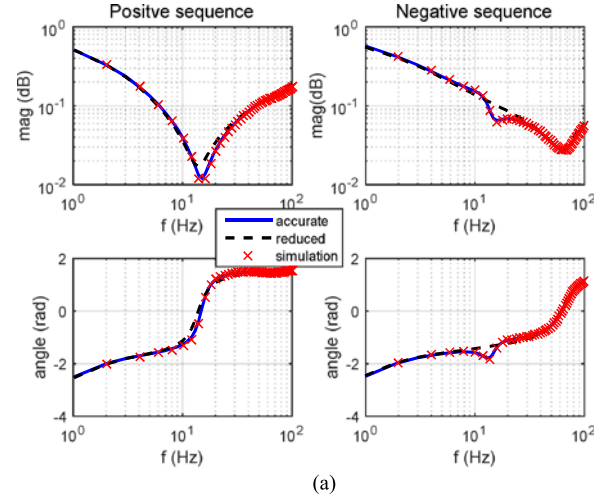


Fig. 7. Loop impedance comparison under dq asymmetric grid. (a) SCR = 4, CC = 200 Hz, PLL = 5 Hz, current is 0.5 p.u. (flow out) (Note that SCR here is only used for calculating grid passive impedance). (b) SCR = 4, CC = 200 Hz, PLL = 300 Hz, current is 0.5 p.u. (flow out) (Note that SCR here is only used for calculating grid impedance).

the measured impedances under a slow PLL configuration. However, if PLL bandwidth is increased to a relatively large value, the shapes of the reduced model would differ from the measurements, particularly for the negative sequence impedances, as shown in Fig. 5(b). By contrast, the accurate SISO model tracks the measured impedances accurately in Fig. 5(b). It proves that the accurate SISO model is superior to the reduced SISO model in capturing the details of impedance characteristics.

2) dq Asymmetric Grid Cases: In this paragraph, an actively controlled grid is introduced to emulate the asymmetric behavior in source subsystem.

The control scheme is shown as below:

In Fig. 6,  $\omega_s = 2\pi \cdot 50$  is constant,  $U_s^{\text{ref}}$  is the voltage amplitude set point of the active grid.  $H_v(s) = k_p^v + \frac{k_v^v}{s}$  is the voltage regulator. The sequence impedance of the actively controlled grid is asymmetric and can be found in Appendix. B ((A.1) and (A.2)).

Comparing Fig. 7(a) with Fig. 6(a) we can identify that, the good accuracy of reduced SISO model under symmetric grid as

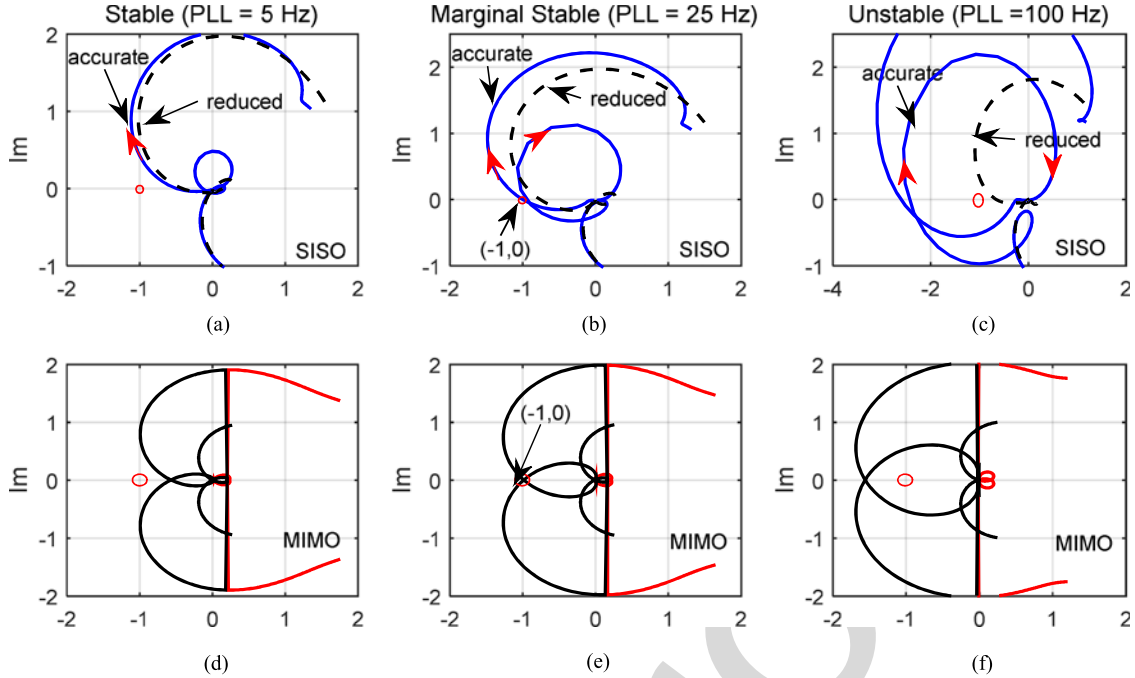


Fig. 8. Numerical stability comparisons with an asymmetric grid (SCR = 4, CC = 200 Hz, current is 0.5 p.u., dash line denotes locus of reduced SISO model, solid blue line denotes locus of accurate SISO model).

311 well as slow PLL configuration is violated if dq asymmetric  
 312 grid is presented. The inaccuracy of reduced SISO model can  
 313 be identified clearly in Fig. 7(b) as well, where a fast PLL is  
 314 adopted. On the contrary, the accurate SISO model still presents  
 315 good accuracy in all conditions.

#### 316 IV. SMALL-SIGNAL STABILITY ANALYSIS

317 This section will further analyze the validity of the proposed  
 318 SISO models in terms of small-signal stability, particularly for  
 319 the marginal stability condition in Section III-C. By acquiring  
 320 the advantages of SISO properties, the proposed model can be  
 321 used in combination with classic Nyquist criterion (NC) [23].

##### 322 A. Numerical Stability Analysis

323 Three model and criterion combinations are considered:

- 324 1) Reduced SISO with NC. (For comparison)
- 325 2) Accurate SISO with NC. (For comparison)
- 326 3) MIMO model with GNC. (For Reference).

327 In a, the eigenvalue loci is obtained straightforward as  
 328  $\lambda_P(s) = \mathbf{Z}_S^{PP} \cdot \mathbf{Y}_L^{PP}$  and  $\lambda_N(s) = \mathbf{Z}_S^{nn} \cdot \mathbf{Y}_L^{PP}$  in accordance with  
 329 (18) and (19).

330 In b, since the SISO loop impedance in (13) can be de-  
 331 composed into source and load subsystems as (15) and (16).  
 332 Therefore, the eigenvalue loci of minor loop gains are  $\lambda_P(s) =$   
 333  $\mathbf{Z}_S^P / \mathbf{Z}_L^P$  and  $\lambda_N(s) = \mathbf{Z}_S^n / \mathbf{Z}_L^P$ , where  $\mathbf{Z}_S^P, \mathbf{Z}_L^P, \mathbf{Z}_S^n, \mathbf{Z}_L^P$  are given  
 334 by (15)–(17).

335 In c, the eigenvalue loci can be calculated from  $\det$   
 336  $|\lambda \cdot \mathbf{I} - \mathbf{Z}_S^{PN} \mathbf{Y}_L^{PN}(s)| = 0$ , where  $\lambda_1(s), \lambda_2(s)$  are the two solu-  
 337 tions. The abovementioned eigenvalue loci are complex transfer  
 338 functions; thus, the locus for negative frequencies is not the

339 conjugation of the locus of positive frequencies [16]. How-  
 340 ever, the eigenvalue loci of SISO systems have the property  
 341  $(\lambda_N(j\omega))^* = \bar{\lambda}_N(-j\omega) = \lambda_P(-j\omega)$ . Hence, the negative fre-  
 342 quency plots can be obtained by conjugating the negative  
 343 sequence locus.

344 Fig. 8 illustrates the stability comparisons of three model and  
 345 criterion combinations under a dq asymmetric grid condition.  
 346 By varying PLL bandwidth in three steps from slow to fast, the  
 347 system is stable, marginal stable and unstable respectively. The  
 348 accurate SISO model with NC has the same stability conclusion  
 349 as the MIMO model with GNC. Particularly, the eigenvalue loci  
 350 of accurate SISO model and MIMO model cross the  $(-1, 0j)$   
 351 point simultaneously, indicating that the proof of marginal sta-  
 352 bility condition in Section III-C is correct. On the other hand,  
 353 the reduced SISO model fails to give the correct marginal sta-  
 354 bility condition, as well as the stability conclusion, identified in  
 355 Figs. 8(b) and (c) respectively.

356 Therefore, it is not safe to use the reduced SISO model if the  
 357 converter and grid is highly dq asymmetric. On the contrary,  
 358 the accurate SISO model is effective for stability analysis in this  
 359 respect.

360 The marginal stability can also be analyzed physically by find-  
 361 ing the damping characteristic at resonances of loop impedance,  
 362 e.g., by passivity analysis in [24]. The following time domain  
 363 study will provide more physical insights into the oscillatory  
 364 behavior lies in the grid-tied VSC system.

##### 365 B. Simulation Study

366 The physical interpretation of marginally stable condition is  
 367 that the loop impedance has approximately zero damping at a  
 368 resonance frequency. By plotting the real and imaginary parts



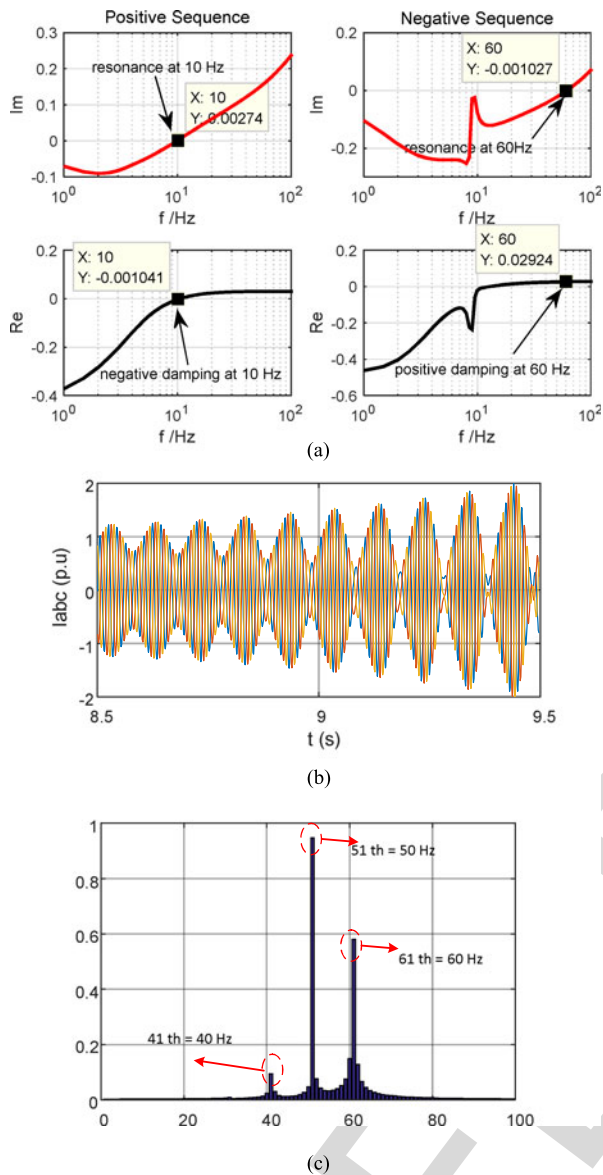


Fig. 9. Marginally stable analysis (CC = 200 Hz SCR = 4, VSC current is 1 p.u.). (a) Positive and negative sequence loop impedance plots. (b) Time domain simulation. (Before 2 seconds, the PLL bandwidth is 5 Hz to achieve a stable operational point. Afterwards, the PLL bandwidth is set to 20 Hz. Oscillation is observable after several seconds.). (c) Fourier analysis of phase current. (Sampling rate is 1 kHz. Sampling window is 1 second.)

of loop impedance, the resonances can be found at frequencies where the imaginary part cross zero axis, meanwhile damping at these resonances can be determined according to the sign of real parts.

As shown in Fig. 9(a), the positive sequence loop impedance has a resonance at 10 Hz, while the negative sequence loop impedance has a resonance at 60 Hz, this findings is consistent with the analytical calculation of resonant points in [22]. Furthermore, the damping at 10 Hz resonance is negative with small value, indicating a marginally unstable condition, on the contrary a positive damping characteristic is presented at 60 Hz, indicating a stable resonance. It is again emphasized that the resonance frequencies are referred to dq frame in the above analysis.

Time domain simulations in PSCAD/EMTDC also draw similar conclusions in terms of stability. The VSC output currents gradually become unstable during a long simulation time in Fig. 9(b), this is due to the fact that negative damping at 10 Hz is small.

Furthermore, by performing a Fourier analysis on the phase current, we can identify that two additional frequencies except the fundamental at 40 Hz and 60 Hz appears, the *mirror frequency coupling effect* is originated from oscillations in dq frame at 10 Hz, which again proves the correctness of above analysis. Additionally, the oscillatory behavior shown in Fig. 9(b) is also similar to the field measurements of grid-tied photovoltaic inverter systems in [25].

## V. CONCLUSION

This paper developed a generalized method for converting dq impedance model of grid-tied VSC system into its SISO sequence domain equivalents. The converting process includes two steps: firstly converts dq impedance into its MIMO sequence domain equivalent, then converts the MIMO sequence domain equivalent into its SISO equivalent by means of closed-loop analysis method proposed in this paper. The decoupled SISO model allows the classic Nyquist Criterion to be used for stability analysis.

Two types of SISO model were given, the accurate one is directly from the consequence of conversion, and the reduced one is derived with a strong grid condition approximation. Numerical and time domain analysis shown that the reduced SISO model gives the wrong stability conclusions in cases where the system is highly dq asymmetric. On the contrary, the accurate SISO model presents a good consistence with MIMO model in terms of stability conclusions, particularly for the marginally stable condition.

The proposed method is general for any MIMO LTI systems. Therefore it is applicable to grid-tied VSC systems where a power controller or DC voltage controller is adopted. Only the marginal stability condition is proven to be identical in this work. Performance on gain and phase margin should be carefully evaluated in future works.

## APPENDIX

### A. Circuit Parameters Used in Stability Analysis and Simulations

TABLE A1  
CIRCUIT PARAMETERS OF THE GRID-TIED VSC SYSTEM

NAME	VALUES	NAME	VALUES
Nominal rating	2 MVA	Filter inductance	0.1 p.u.
Nominal voltage	0.69 kV	Grid inductance (SCR = 4)	1/SCR = 0.25 p.u.
Dc voltage	1.1 kV	Current controller (CC = 200 Hz)	$k_p^c = 0.03, k_i^c = 6.1$
Switching frequency	2.4 kHz	PLL controller (PLL = 20 Hz)	$k_p^{pll} = 71, k_i^{pll} = 1421$
		asymmetric grid controller	$k_p^v = 1, k_i^v = 100$

## 424 B. Modeling of Actively Controlled Grid

425 The dq domain grid model with control scheme in Fig. 6 is:

$$\mathbf{Z}_{\text{grid}}^{\text{dq}}(s) = \begin{bmatrix} 1 + \cos \delta_0 H_V(s) & 0 \\ -\sin \delta_0 H_V(s) & 1 \end{bmatrix} \begin{bmatrix} sL_s + R_s & -\omega_s L_s \\ \omega_s L_s & sL_s + R_s \end{bmatrix} \quad (\text{A.1})$$

426 where  $\delta_0$  is the steady voltage angle difference between PCC and  
427 grid. Clearly, the dq impedance of actively controlled grid is  
428 not symmetric. Using the decomposition method in Section II-B  
429 gives a coupled sequence impedance:

$$\mathbf{Z}_{\text{grid}}^{\text{PN}}(s) = \mathbf{A} \mathbf{Z}_{\text{grid}}^{\text{dq}}(s) \mathbf{A}^{-1} \quad (\text{A.2})$$

## 430 C. dq Symmetric and Asymmetric

431 For a dq impedance matrix  $\begin{bmatrix} Z^{\text{dd}}(s) & Z^{\text{dq}}(s) \\ Z^{\text{qd}}(s) & Z^{\text{qq}}(s) \end{bmatrix}$ , it is said to be  
432 dq symmetric if  $Z^{\text{dd}}(s) = Z^{\text{qq}}(s)$  and  $Z^{\text{dq}}(s) = -Z^{\text{qd}}(s)$ , and  
433 if the condition not satisfied, the system is referred to dq asym-  
434 metric. For a dq symmetric system, its sequence equivalent  
435 can be obtained by linear transformation using the methods in  
436 Section II. As a result, the sequence impedance is decoupled.  
437 Otherwise, the sequence impedance is coupled.

## 438 REFERENCES

- 439 [1] R. Teodorescu, M. Liserre, and P. Rodriguez, "Introduction," in *Grid*  
440 *Converters for Photovoltaic and Wind Power Systems*. Chichester, U.K.:  
441 Wiley, 2011, pp. 1–4.  
442 [2] N. Flourentzou, V. G. Agelidis, and G. D. Demetriades, "VSC-Based  
443 HVDC power transmission systems: An overview," *IEEE Trans. Power*  
444 *Electron*, vol. 24, no. 3, pp. 592–602, Mar. 2009.  
445 [3] D. Dong, B. Wen, D. Boroyevich, P. Mattavelli, and Y. Xue, "Analysis of  
446 phase-locked loop low-frequency stability in three-phase grid-connected  
447 power converters considering impedance interactions," *IEEE Trans. Ind.*  
448 *Electron.*, vol. 62, no. 1, pp. 310–321, Jan. 2015.  
449 [4] L. P. Kunjumammed, B. C. Pal, C. Oates, and K. J. Dyke, "Electrical  
450 oscillations in wind farm systems: Analysis and insight based on detailed  
451 modeling," *IEEE Trans. Sustain. Energy*, vol. 7, no. 1, pp. 51–62, Jan.  
452 2015.  
453 [5] D. Yang, X. Ruan, and H. Wu, "Impedance shaping of the grid-connected  
454 inverter with LCL filter to improve its adaptability to the weak grid condi-  
455 tion," *IEEE Trans. Power Electron*, vol. 29, no. 11, pp. 5795–5805, Nov.  
456 2014.  
457 [6] L. Harnefors, M. Bongiorno, and S. Lundberg, "Input-admittance calcu-  
458 lation and shaping for controlled voltage-source converters," *IEEE Trans.*  
459 *Ind. Electron.*, vol. 54, no. 6, pp. 3323–3334, Dec. 2007.  
460 [7] M. Belkhat, "Stability criteria for AC power systems with regulated  
461 loads," Ph.D. dissertation, Purdue University, West Lafayette, IN, USA,  
462 1997.  
463 [8] M. Cespedes and J. Sun, "Impedance modeling and analysis of grid-  
464 connected voltage-source converters," *IEEE Trans. Power Electron.*,  
465 vol. 29, no. 3, pp. 1254–1261, Mar. 2014.  
466 [9] B. Wen, D. Boroyevich, R. Burgos, P. Mattavelli, and Z. Shen, "Small-  
467 signal stability analysis of three-phase AC systems in the presence of  
468 constant power loads based on measured d-q, frame impedances," *IEEE*  
469 *Trans. Power Electron.*, vol. 30, no. 10, pp. 5952–5963, Oct. 2015.  
470 [10] S. Shah and L. Parsa, "On impedance modeling of single-phase voltage  
471 source converters," in *Proc. IEEE Energy Convers. Congr. Expo.*, 2016,  
472 pp. 1–8.  
473 [11] J. Lyu, X. Cai, and M. Molinas, "Impedance modeling of modular  
474 multilevel converters," in *Proc. Annu. Conf. IEEE Ind. Electron. Soc.*,  
475 Yokohama, Japan, 2015, pp. 180–185.

- [12] J. Sun, "Small-signal methods for AC distributed power systems—A review," in *Proc. IEEE Electr. Ship Technol. Symp.*, 2009, pp. 44–52. 476  
477  
[13] E. Möllerstedt, "Dynamic analysis of harmonics in electrical systems," 478  
Ph.D. dissertation, Dept. Automat. Control, Lund University, Lund, 479  
Sweden, 2000. 480  
[14] M. K. Bakhshizadeh *et al.*, "Couplings in phase domain impedance mod- 481  
eling of grid-connected converters," *IEEE Trans. Power Electron*, vol. 31, 482  
no. 10, pp. 6792–6796, Oct. 2016. 483  
[15] S. Shah and L. Parsa, "Sequence domain transfer matrix model of three- 484  
phase voltage source converters," in *Proc. IEEE Power Energy Soc. Gener- 485  
al Meet.*, 2016, pp. 1–5. 486  
[16] L. Harnefors, "Modeling of three-phase dynamic systems using com- 487  
plex transfer functions and transfer matrices," *IEEE Trans. Ind. Electron*, 488  
vol. 54, no. 4, pp. 2239–2248, Aug. 2007. 489  
[17] A. Rygg, M. Molinas, C. Zhang, and X. Cai, "A modified sequence domain 490  
impedance definition and its equivalence to the dq-domain impedance 491  
definition for the stability analysis of ac power electronic systems," *IEEE* 492  
*J. Emerg. Sel. Topics Power Electron.*, vol. 4, no. 4, pp. 1382–1396, Dec. 493  
2016. 494  
[18] G. C. Paap, "Symmetrical components in the time domain and their appli- 495  
cation to power network calculations," *IEEE Trans. Power Syst*, vol. 15, 496  
no. 2, pp. 522–528, May 2000. 497  
[19] X. Wang, L. Harnefors, F. Blaabjerg, and P.C. Loh, "A unified impedance 498  
model of voltage-source converters with phase-locked loop effect," in 499  
*Proc. IEEE Energy Convers. Congr. Expo.*, 2016, pp. 1–8. 500  
[20] J. Kwon, X. Wang, F. Blaabjerg, C. L. Bak, V. S. Sularea, and C. Busca, 501  
"Harmonic interaction analysis in grid-connected converter using Har- 502  
monic State Space (HSS) modeling," *IEEE Trans. Power Electron.*, vol. 32, 503  
no. 9, pp. 6823–6835, Sep. 2016. 504  
[21] C. Desoer and Y.T. Wang, "On the generalized nyquist stability crite- 505  
rion," *IEEE Trans. Autom. Control*, vol. 25, no. 2, pp. 187–196, Apr. 506  
1980. 507  
[22] C. Zhang, X. Cai, Z. Li, A. Rygg, and M. Molinas, "Properties and phys- 508  
ical interpretation of the dynamic interactions between voltage source 509  
converters and grid: Electrical oscillation and its stability control," *IET* 510  
*Power Electron.*, vol. 10, no. 8, pp. 894–902, Jun. 2017. 511  
[23] J. Sun, "Impedance-based stability criterion for grid-connected invert- 512  
ers," *IEEE Trans. Power Electron*, vol. 26, no. 11, pp. 3075–3078, Nov. 513  
2011. 514  
[24] L. Harnefors, X. Wang, A. G. Yepes, and F. Blaabjerg, "Passivity-based 515  
stability assessment of grid-connected VSCs—An overview," *IEEE J.* 516  
*Emerg. Sel. Topics Power Electron.*, vol. 4, no. 1, pp. 116–125 Mar. 517  
2016. 518  
[25] C. Li, "Unstable operation of photovoltaic inverter from field experiences," 519  
*IEEE Trans. Power Del.*, to be published. 520



aim is to reveal the fundamental dynamics and stability mechanisms of renewable energies with VSCs as the grid interface.

**Chen Zhang** received the B.Eng. degree in electrical engineering from China University of Mining and Technology, Xuzhou, China, in 2011. He is currently working toward the Ph.D. degree in electrical engineering with Shanghai Jiao Tong University, Shanghai, China. He was a Ph.D. Visiting Scholar in the Department of Engineering Cybernetics, Norwegian University of Science and Technology, Trondheim, Norway, in 2015. His current research interests include modeling and stability analysis of VSC-based energy conversion systems, where the

476  
477  
478  
479  
480  
481  
482  
483  
484  
485  
486  
487  
488  
489  
490  
491  
492  
493  
494  
495  
496  
497  
498  
499  
500  
501  
502  
503  
504  
505  
506  
507  
508  
509  
510  
511  
512  
513  
514  
515  
516  
517  
518  
519  
520  
Q2



535  
536  
537  
538  
539  
540  
541  
542  
543  
544  
545  
546  
547  
548  
549  
550  
551



**Xu Cai** received the B.Eng. degree from Southeast University, Nanjing, China, in 1983, and the M.Sc. and Ph.D. degrees from China University of Mining and Technology, Xuzhou, China, in 1988 and 2000, respectively. He was in the Department of Electrical Engineering, China University of Mining and Technology, as an Associate Professor, from 1989 to 2001. He was the Vice Director of the State Energy Smart Grid R&D Center, Shanghai, China, from 2010 to 2013. He has been with Shanghai Jiao Tong University, Shanghai, as a Professor, since 2002, where he

has also been the Director of the Wind Power Research Center, since 2008. His current research interests include power electronics and renewable energy exploitation and utilization, including wind power converters, wind turbine control system, large power battery storage systems, clustering of wind farms and its control system, and grid integration.

552  
553  
554  
555  
556  
557  
558  
559  
560  
561  
562  
563



**Atle Rygg** received the M.Sc. degree in electrical engineering from Norwegian University of Science and Technology (NTNU), Trondheim, Norway, in 2011. He is currently working toward the Ph.D. degree in Department of Engineering Cybernetics at NTNU. From 2011 to 2015, he was a Research Scientist at SINTEF Energy Research in the field of power electronics. His topic or research interests include impedance based stability analysis of power electronic systems, where the aim is to contribute to the fundamental understanding in this family of methods.



**Marta Molinas** (M'94) received the Diploma degree in electromechanical engineering from the National University of Asuncion, Asuncion, Paraguay, in 1992, the Master of Engineering degree from Ryukyu University, Nishihara, Japan, in 1997, and the Doctor of Engineering degree from Tokyo Institute of Technology, Tokyo, Japan, in 2000. She was a Guest Researcher with the University of Padova, Padova, Italy, during 1998. From 2004 to 2007, she was a Postdoctoral Researcher with the Norwegian University of Science and Technology (NTNU) and

from 2008 to 2014 she has been Professor in the Department of Electric Power Engineering at the same university. She is currently a Professor in the Department of Engineering Cybernetics, NTNU. Her research interests include stability of power electronics systems, harmonics, instantaneous frequency, and nonstationary signals from the human and the machine. She is an Associate Editor for the IEEE JOURNAL OF EMERGING AND SELECTED TOPIC IN POWER ELECTRONICS, the IEEE TRANSACTIONS ON POWER ELECTRONICS and an Editor of the IEEE TRANSACTIONS ON ENERGY CONVERSION. She has been an AdCom Member of the IEEE Power Electronics Society from 2009 to 2011.

564  
565  
566  
567  
568  
569  
570  
571  
572  
573  
574  
575  
576  
577  
578  
579  
580  
581  
582  
583  
584

IEEE PROCEEDINGS

- 586 Q1. Author: Please provide the department name in Ref. [7].  
587 Q2. Author: Please update Ref. [25].

IEEE Proof

# Sequence Domain SISO Equivalent Models of a Grid-Tied Voltage Source Converter System for Small-Signal Stability Analysis

Chen Zhang, Xu Cai, Atle Rygg, and Marta Molinas, *Member, IEEE*

**Abstract**—This paper presents a generalized method for converting multi-input and multi-output (MIMO)  $dq$  impedance model of a grid-tied voltage source converter system into its sequence domain single-input and single-output (SISO) equivalents. As a result, two types of SISO impedance models were derived, one of which was derived from relatively strong and  $dq$  symmetric grid assumption (reduced SISO model) and the other was based on closed-loop equivalent (accurate SISO model). It was proven that the accurate SISO model has the same marginal stability condition as the MIMO model. Accuracy of these models is assessed with respect to the measured impedances in PSCAD/EMTDC simulations, their effects on stability are analyzed as well. Findings show that the accurate SISO model presents identical stability conclusions as the MIMO model. However, the reduced SISO model may lead to inaccurate results if the system is highly  $dq$  asymmetric, e.g., VSC with fast phase-locked loop or an actively controlled grid.

**Index Terms**—Couplings, PLL, sequence impedance, stability analysis, voltage source converter.

## I. INTRODUCTION

NOWADAYS, voltage source converters (VSC) have become widely used in grid-integrated renewable energies [1] and flexible power transmission systems [2]. Oscillations at both low [3] and high frequencies [4] were observed in VSC-based systems, particularly in weak grid conditions [5]. Such types of small-signal stability issues can be effectively assessed by impedance-based analysis. Impedance models of three-phase VSCs [6]–[9], single-phase VSCs [10], and modular multi-level converters [11], among others, have been developed rigorously in recent literature.

For typical two-level and three-phase grid-tied VSCs, the impedance can be extracted either in  $dq$  synchronously rotating frame [7] or in three-phase stationary frame [8]. In  $dq$

Manuscript received April 24, 2017; revised July 9, 2017 and September 5, 2017; accepted October 18, 2017. This work was supported by grants from the Power Electronics Science and Education Development Program of the Delta Environmental and Educational Foundation (DREM2016005). Paper no. TEC-00310-2017. (*Corresponding author: Chen Zhang.*)

C. Zhang and X. Cai are with the Department of Electrical Engineering, Shanghai Jiao Tong University, Shanghai 200240, China (e-mail: nealbc@sjtu.edu.cn; xucai@sjtu.edu.cn).

A. Rygg and M. Molinas are with the Department of Engineering Cybernetics, Norwegian University of Science and Technology, Trondheim 7491, Norway (e-mail: atle.rygg@ntnu.no; marta.molinas@ntnu.no).

Color versions of one or more of the figures in this paper are available online at <http://ieeexplore.ieee.org>.

Digital Object Identifier 10.1109/TEC.2017.2766217

frame, the grid-tied VSC system is time invariant if grid is three-phase balanced. This setup allows for direct linearization; thus, performing Laplace transformation on the resultant linear time invariant (LTI) model yields  $dq$  impedances [9]. However, if applied to three-phase stationary frame, the grid-tied VSC inherently varies by time. Therefore, the harmonic linearization method from a previous study [12] is applied to obtain sequence impedances [8]. Generally, linearizing the time-varying system along a steady periodic trajectory yields a linear time periodic (LTP) system. To transform LTP systems into frequency domain, the harmonic balance approach [13] can be adopted.

Despite the different models in  $dq$  and sequence domains, both are coupled because of the off-diagonal terms in impedance matrices are nonzero. Recent research has presented interest in the interpretation of these couplings and their consequences during stability assessment. Previous works [14], [15] established that frequency couplings can be identified in their sequence domain (i.e., positive and negative sequences are coupled and separated by twice fundamental frequency); and their impacts on low-frequency stability were also emphasized. This interesting property of VSC was also identified from  $dq$  impedance and introduced as  $dq$  asymmetry in [16]. Moreover, the relationship between  $dq$  and sequence impedances were thoroughly investigated in [17], and findings showed that  $dq$  impedances can be transformed into its modified sequence domain equivalents by means of symmetrical decomposition [18]. On the other hand, a complex space vector method [16] is used to directly derive VSC impedance in stationary frame [19].

However, frequency couplings in the foregoing reviews (e.g., [14]–[17]) were in single-frequency coupling form (i.e., a single-frequency perturbation induces a single-frequency coupling that separated by twice the fundamental frequency). This condition is true if either the converter or the grid impedance is  $dq$  asymmetric [16] or equivalently contains the mirror frequency coupling effect [17]. If the system is three-phase unbalanced, there will be multiple frequency couplings. To include these couplings with full accuracy, the harmonic-state space [20] as well as the harmonic transfer function method [13] should be adopted.

Currently, both cases on single- and multiple-frequency couplings can only be captured by matrix-based impedances, which are multi-input and multi-output (MIMO) systems by nature; therefore, the generalized Nyquist criterion (GNC) [21] should be adopted for stability analysis. Furthermore, finding the



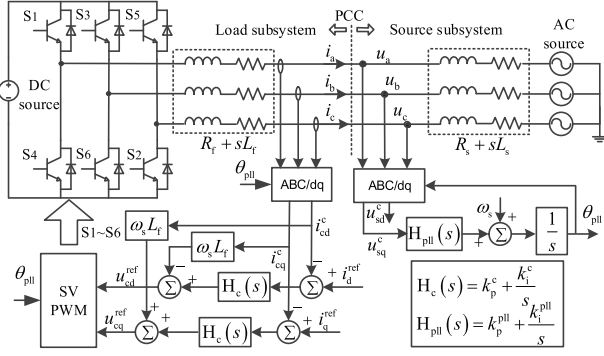


Fig. 1. Schematic of the grid-tied VSC system.

81 single-input and single-output (SISO) equivalents of grid-tied  
82 VSC system is appealing due to their simplicity and convenience  
83 for physical interpretation.

84 This paper aims to develop a generalized method for con-  
85 verting MIMO dq impedance into its sequence domain SISO  
86 equivalents by exploring the properties of single-frequency cou-  
87 pling system. The rest of the paper is organized as follows: In  
88 Section II, the method for converting the dq impedance into  
89 its MIMO sequence domain equivalents is introduced. System  
90 blocks of a grid-tied VSC system are modeled based on this  
91 method. In Section III, sequence domain MIMO model of grid-  
92 tied VSC system is established by assembling the blocks in  
93 Section II. And its SISO equivalents are found by performing  
94 closed-loop analysis of the entire system, instead of viewing  
95 them as subsystems. A detailed comparison of SISO models  
96 with measured impedances in PSCAD/EMTDC is presented.  
97 Section IV discussed the performance of proposed SISO mod-  
98 els in predicting small signal stability. Finally, Section V draws  
99 the conclusions.

## 100 II. MODELING OF GRID-TIED VSC IN MODIFIED 101 SEQUENCE DOMAIN

### 102 A. Topology and Control Scheme of the Grid-Tied VSC

103 Fig. 1 presents the system analyzed in this paper. It consti-  
104 tutes a typical two-level VSC, an L-type filter, and a Thevenin-  
105 equivalent grid.

106 Only current controller and phase-locked loop (PLL) are con-  
107 sidered, mainly to achieve simplicity of subsequent property  
108 analysis. It will not affect the generality of proposed method  
109 as will be presented later. Grid voltage feedforwards can have  
110 a great impacts on both transient [6] and small-signal response  
111 [5] of VSC, if the bandwidths of these feedforwards are not  
112 carefully chosen. In this regard, feedforwards are viewed as  
113 impedance-shaping method, and will not be discussed in this  
114 paper because the focus is on modeling.

### 115 B. Symmetrical Decomposition of a dq Impedance

116 Taking a dq impedance model in [9] as an example,

$$\begin{bmatrix} U_d(s) \\ U_q(s) \end{bmatrix} = \begin{bmatrix} Z^{dd}(s) & Z^{dq}(s) \\ Z^{qd}(s) & Z^{qq}(s) \end{bmatrix} \begin{bmatrix} I_d(s) \\ I_q(s) \end{bmatrix} \quad (1)$$

Expression (1) is a LTI system and a complex exponential  
input (e.g.,  $e^{st}$ ) leads to an output with the same formation [13].  
Thus, the variables for dq currents and voltages in (1) can be  
written explicitly with variable  $s$ , as shown below.

$$\begin{bmatrix} U_d \\ U_q \end{bmatrix} e^{st} = \begin{bmatrix} Z^{dd}(s) & Z^{dq}(s) \\ Z^{qd}(s) & Z^{qq}(s) \end{bmatrix} \begin{bmatrix} I_d \\ I_q \end{bmatrix} e^{st}, \forall s \rightarrow j\omega \quad (2)$$

where  $s \rightarrow j\omega$  is translated from  $s$ -domain to frequency-domain.  
 $I_d, I_q$  and  $U_d, U_q$  are the current and voltage phasors at fre-  
quency  $\omega$  respectively, and they can be decomposed as:

$$\begin{bmatrix} U_p \\ U_n \end{bmatrix} = \frac{1}{2} \begin{bmatrix} 1 & j \\ 1 & -j \end{bmatrix} \begin{bmatrix} U_d \\ U_q \end{bmatrix} = \mathbf{A} \begin{bmatrix} U_d \\ U_q \end{bmatrix} \quad (3)$$

Applying matrix  $\mathbf{A}$  and its inverse  $\mathbf{A}^{-1}$  to (2) yields:

$$\begin{bmatrix} U_p \\ U_n \end{bmatrix} = \mathbf{A} \begin{bmatrix} Z^{dd}(s) & Z^{dq}(s) \\ Z^{qd}(s) & Z^{qq}(s) \end{bmatrix} \mathbf{A}^{-1} \begin{bmatrix} I_p \\ I_n \end{bmatrix} \\ = \mathbf{Z}^{PN}(s) \begin{bmatrix} I_p \\ I_n \end{bmatrix}, \forall s \rightarrow j\omega \quad (4)$$

where elements in  $\mathbf{Z}^{PN}(s) = \begin{bmatrix} Z^{dd}(s) & Z^{dq}(s) \\ Z^{qd}(s) & Z^{qq}(s) \end{bmatrix}$  are generally com-  
plex transfer functions. This method makes it possible to obtain  
the modified sequence impedance directly from well-developed  
dq impedance as discussed in [17] (i.e., the same authors of this  
paper). The term ‘‘modified’’ denotes the specific frequency nota-  
tion used in [17], where the frequency of sequence impedances  
is referred to dq frame. This notation is adopted in the present  
paper as well, and the term ‘‘modified’’ will be omitted for brevity  
in subsequent analysis. However, other recent works e.g., [14]  
and [19] use a different frequency notation, which are referred  
to phase domain.

### 103 C. Sequence Domain System Blocks of Grid-Tied VSC

104 Adopting the decomposition method in Section II-B, system  
105 blocks of a grid-tied VSC system in dq format (e.g., [9]) can  
106 be transformed into their sequence domain equivalents.

For passive circuit elements, e.g., filter:

$$\begin{bmatrix} R_f + sL_f & -\omega_s L_f \\ \omega_s L_f & R_f + sL_f \end{bmatrix} \xrightarrow{\text{dq-pn}} \begin{bmatrix} Z_f^{pp}(s) & 0 \\ 0 & Z_f^{nn}(s) \end{bmatrix} \quad (5)$$

where  $Z_f^{pp}(s) = R_f + sL_f + j\omega_s L_f$ ,  $Z_f^{nn}(s) = \bar{Z}_f^{pp}(s)$ . The up-  
per line on the latter denotes complex-conjugate operator on  
the function (i.e., the coefficients not the Laplace variable ‘‘s’’).  
For a typical Thevenin grid, its sequence impedances are simi-  
larly as the filter, which are  $Z_s^{pp}(s) = R_s + sL_s + j\omega_s L_s$  and  
 $Z_s^{nn}(s) = \bar{Z}_s^{pp}(s)$  respectively.

For variables perturbed by abc to dq transformation e.g.,  
converter output currents:

$$\begin{bmatrix} 0 & \frac{I_{c0} T_{pll}(s)}{U_0} \\ 0 & -\frac{I_{cd0} T_{pll}(s)}{U_0} \end{bmatrix} \xrightarrow{\text{dq-pn}} \frac{T_{pll}(s)}{2U_0} \begin{bmatrix} -I_{c0} & I_{c0} \\ I_{c0}^* & -I_{c0}^* \end{bmatrix} \quad (6)$$

where  $T_{pll}(s) = \frac{U_0 H_{pll}(s)}{s + U_0 H_{pll}(s)}$  is the closed-loop system of a  
typical PLL as in Fig. 1.  $U_0$  is the voltage at PLL sampling point.

151  $\underline{I}_{c0} = I_{cd0} + jI_{cq0}$  is the complex-valued current in steady.  
 152 The converter output voltage can be obtained similarly as:  
 153  $\frac{T_{pll}(s)}{2U_0} \begin{bmatrix} -\underline{U}_{c0} & \underline{U}_{c0} \\ \underline{U}_{c0} & -\underline{U}_{c0}^* \end{bmatrix} \cdot \underline{U}_{c0} = U_{cd0} + jU_{cq0}$  is the complex-valued  
 154 converter terminal voltage.

155 For current controller it has:

$$\begin{bmatrix} H_c(s) & 0 \\ 0 & H_c(s) \end{bmatrix} \xrightarrow{\text{dq-pn}} \begin{bmatrix} H_c^{pp}(s) & 0 \\ 0 & H_c^{nn}(s) \end{bmatrix} \quad (7)$$

156 Generally, all the system blocks in dq domain can be trans-  
 157 formed into their sequence domain equivalents, e.g., VSC with  
 158 PQ controller, DC voltage controller etc.

#### 159 D. Sequence Impedance Model of the Grid-Tied VSC System

160 The sequence domain MIMO model of a grid-tied VSC sys-  
 161 tem can be established by assembling system blocks derived in  
 162 Section II-C.

163 For a load (VSC) subsystem, its admittance is:

$$-\begin{bmatrix} \mathbf{i}_L^p \\ \mathbf{i}_L^n \end{bmatrix} = \begin{bmatrix} \mathbf{Y}_L^{pp}(s) & \mathbf{Y}_L^{pn}(s) \\ \mathbf{Y}_L^{np}(s) & \mathbf{Y}_L^{nn}(s) \end{bmatrix} \begin{bmatrix} \mathbf{u}_L^p \\ \mathbf{u}_L^n \end{bmatrix} = \mathbf{Y}_L^{PN}(s) \begin{bmatrix} \mathbf{u}_L^p \\ \mathbf{u}_L^n \end{bmatrix} \quad (8)$$

164 For a generalized source (grid) subsystem, its impedance is:

$$\begin{bmatrix} \mathbf{u}_S^p \\ \mathbf{u}_S^n \end{bmatrix} = \begin{bmatrix} \mathbf{Z}_S^{pp}(s) & \mathbf{Z}_S^{pn}(s) \\ \mathbf{Z}_S^{np}(s) & \mathbf{Z}_S^{nn}(s) \end{bmatrix} \begin{bmatrix} \mathbf{i}_S^p \\ \mathbf{i}_S^n \end{bmatrix} = \mathbf{Z}_S^{PN}(s) \begin{bmatrix} \mathbf{i}_S^p \\ \mathbf{i}_S^n \end{bmatrix} \quad (9)$$

$$\mathbf{i}_S^p = \mathbf{i}_L^p, \mathbf{i}_S^n = \mathbf{i}_L^n \quad (10)$$

$$\mathbf{u}_S^p + \mathbf{u}_{ptb}^p = \mathbf{u}_L^p, \mathbf{u}_L^n = \mathbf{u}_S^n \quad (11)$$

165 where  $\mathbf{Y}_L^{pp} = \frac{1-G_{pll}}{H_c^{pp} + Z_f^{pp}}$ ,  $\mathbf{Y}_L^{nn} = \bar{\mathbf{Y}}_L^{pp}$ ,  $\mathbf{Y}_L^{pn} = \frac{G_{pll}}{H_c^{pp} + Z_f^{pp}}$ ,  $\mathbf{Y}_L^{np} =$   
 166  $\bar{\mathbf{Y}}_L^{pn}$  and  $G_{pll} = \frac{T_{pll}(s)}{2U_0} (H_c I_{c0} + \underline{U}_{c0})$ . Laplace variable  $s$  is omit-  
 167 ted for brevity.

168  $\mathbf{u}_{ptb}^p$  is a positive sequence perturbation voltage. Functions in  
 169 bold format e.g.,  $\mathbf{Z}_S^{PN}$  denotes a matrix, in the case of Fig. 1, it  
 170 has  $\mathbf{Z}_S^{pn}(s) = \mathbf{Z}_S^{np}(s) = 0$ , as the grid is passive and dq sym-  
 171 metric. The subscript ‘S’ in capital format denotes source (e.g.,  
 172 grid) subsystem, and ‘L’ denotes load (e.g., VSC) subsystem.  
 173 Note that the line on the letter e.g.,  $\bar{\mathbf{Y}}_L^{pp}$  is conjugate operator on  
 174 the function, if the full complex conjugate operator “\*” is used,  
 175 it has  $(\mathbf{Y}_L^{pp})^* = \bar{\mathbf{Y}}_L^{pp}(\bar{s})$ . The derived MIMO model as (8) and  
 176 (9) can be used directly to assess small-signal stability with the  
 177 help of GNC [14]. A previous study [17] proved that the GNC  
 178 based on this model leads to identical results, as the GNC based  
 179 on dq impedance.

180 The sequence equivalent circuits can be plotted as Fig. 2 on  
 181 the basis of (8)–(11). In Fig. 2, positive and negative sequence  
 182 circuits are coupled via two dependent current sources, which  
 183 are voltage controlled. This intrinsic binding between positive  
 184 and negative sequence circuits will be explored further in next  
 185 section for finding their SISO equivalents.

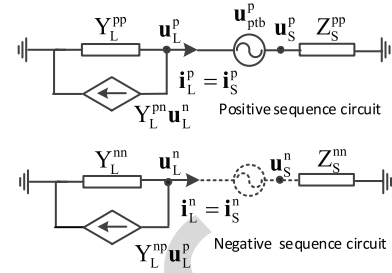


Fig. 2. Sequence domain equivalent circuits of the grid-tied VSC system.

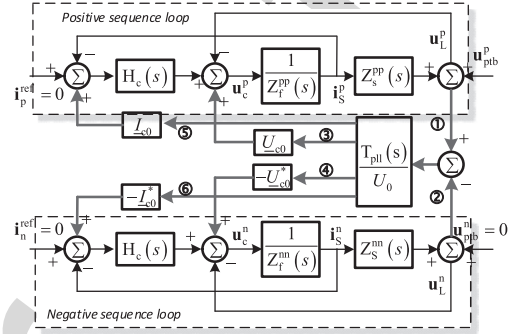


Fig. 3. Sequence domain control blocks diagram of a grid-tied VSC system.

### III. SISO EQUIVALENT MODELS OF A GRID-TIED VSC SYSTEM

#### A. Analysis of Coupled Sequence Loops

In order to reveal the sequence coupling in a more intuitive way, manipulating the system blocks (5)–(7) with electrical system configuration in Fig. 1 yields the following diagram.

Fig. 3 clearly identifies the positive and negative sequence loops coupled via six paths, which are all caused by the PLL (i.e.,  $T_{pll}(s)$ ). Different paths will result in models with different accuracies, as in the following cases:

*Case 1:* By neglecting all paths, the simplest model with decoupled positive and negative sequences is obtained. Although this case may not be effective for stability analysis, it is useful for identifying the intrinsic properties of the grid-VSC system (e.g., resonant point), and the coupling effects of PLL can be introduced as additional damping sources to the intrinsic resonant point [22].

*Case 2:* By isolating the paths of ①③⑤ and ②④⑥, another popular decoupled sequence model as in [8] is obtained. The positive and negative loop impedance from perturbation voltage to the current response can be calculated directly from Fig. 3; i.e.,  $1/\mathbf{Y}_L^{pp} + \mathbf{Z}_S^{pp}$  and  $1/\mathbf{Y}_L^{nn} + \mathbf{Z}_S^{nn}$ . Note that the obtained loop impedance is equivalent to neglect the off-diagonal terms in the converter admittance. This condition is satisfied if the grid is relatively strong and dq symmetric. See the proof in the subsequent analysis as in (18), (19).

The foregoing analysis presents two decoupled models for the grid-tied VSC, which are SISO systems. However, both models neglect sequence coupling to some extent. In the following section, we will develop a method for deriving an accurate SISO model with no assumptions and reductions.

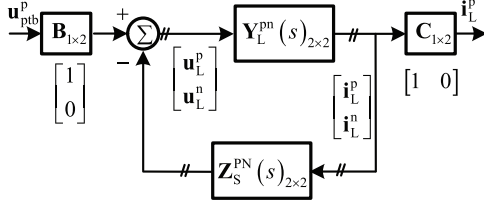


Fig. 4. Closed-loop representation of a grid-tied VSC system.

## B. Accurate and Reduced SISO Models of the Grid-Tied VSC

In this subsection, we regard VSC and grid as a closed-loop system, not as subsystems, perturbed by independent sources. Due to linearity, closed-loop analysis under positive and negative independent perturbations can be analyzed separately.

Taking the positive sequence as an example, the positive sequence loop impedance can be obtained by solving the linear system in Fig. 4:

$$Z_{L_{loop}}^P(s) = -\frac{\mathbf{u}_{ptb}^p}{\mathbf{i}_L^p} = \frac{1}{\mathbf{C}(\mathbf{Z}_L^{\text{PN}}(s) + \mathbf{Z}_S^{\text{PN}}(s))^{-1}\mathbf{B}} \quad (12)$$

where  $\mathbf{Z}_L^{\text{PN}}(s) = (\mathbf{Y}_L^{\text{PN}}(s))^{-1}$ . It should be noted that the derived loop impedance is one dimension, i.e., a SISO system.

Substituting elements as in (8) and (9) into (12) yields:

$$Z_{L_{loop}}^P(s) = Z_S^{\text{PP}} + Z_L^{\text{PP}} - \frac{(Z_L^{\text{NP}} + Z_S^{\text{NP}})(Z_L^{\text{PN}} + Z_S^{\text{PN}})}{Z_S^{\text{NN}} + Z_L^{\text{NN}}} \quad (13)$$

This method is applied to find the negative sequence loop impedance. Replacing the matrix  $\mathbf{B} = [0 \ 1]^T$ ,  $\mathbf{C} = [0 \ 1]$  and  $\mathbf{u}_{ptb}^p \rightarrow \mathbf{u}_{ptb}^n$  yields:

$$Z_{L_{loop}}^N(s) = Z_S^{\text{NN}} + Z_L^{\text{NN}} - \frac{(Z_L^{\text{NP}} + Z_S^{\text{NP}})(Z_L^{\text{PN}} + Z_S^{\text{PN}})}{Z_S^{\text{PP}} + Z_L^{\text{PP}}} \quad (14)$$

Expressions (13) and (14) is defined as the *accurate SISO model*, and  $Z_{L_{loop}}^P(s) = \bar{Z}_{L_{loop}}^N(s)$  still holds, i.e., if we have the analytical model of the positive sequence, the negative sequence model is determined accordingly. In addition, during the derivation, no assumption for dq symmetry was made, therefore this method is general for any LTI systems.

The physical interpretation of this method is: the negative sequence circuit in Fig. 2 is augmented into the positive sequence network (and vice versa) via the voltage-controlled dependent current source. Consequently, the effects of sequence coupling are included in this model intrinsically.

In order to proof the validity of the method, a previous work in [17], where the sequence impedance is derived for source and load subsystem is compared. Taking the positive sequence model for example, in [17] it has:

$$Z_L^P = -\frac{\mathbf{u}_L^p}{\mathbf{i}_L^p} = Z_L^{\text{PP}} - \frac{Z_L^{\text{PN}}(Z_L^{\text{NP}} + Z_S^{\text{NP}})}{Z_S^{\text{NN}} + Z_L^{\text{NN}}} \quad (15)$$

$$Z_S^P = \frac{\mathbf{u}_S^p}{\mathbf{i}_S^p} = Z_S^{\text{PP}} - \frac{Z_S^{\text{PN}}(Z_L^{\text{NP}} + Z_S^{\text{NP}})}{Z_S^{\text{NN}} + Z_L^{\text{NN}}} \quad (16)$$

$$Z_L^N(s) = \bar{Z}_L^P(s)$$

$$Z_S^N(s) = \bar{Z}_S^P(s) \quad (17)$$

We can clearly observe that  $Z_L^P + Z_S^P = Z_{L_{loop}}^P$  and  $Z_L^N + Z_S^N = Z_{L_{loop}}^N$ . ((15) and (16) are equivalent to (33) in [17], but are written in a more compact form with slightly different notation.)

Furthermore, if considering a dq symmetric and relatively strong grid, it has conditions as:  $Z_S^{\text{PP}} = Z_S^{\text{NN}} = 0, |Z_S^{\text{PP}}| \ll |Z_L^{\text{PP}}|, \forall \omega$  and  $|Z_S^{\text{NN}}| \ll |Z_L^{\text{NN}}|, \forall \omega$ . Hence, (13) and (14) can be reduced to:

$$Z_{L_{loop}}^{\text{P,rd}}(s) = Z_S^{\text{PP}} + \frac{\det |Z_L^{\text{PN}}|}{Z_L^{\text{NN}}} = Z_S^{\text{PP}} + \frac{1}{Y_L^{\text{PP}}} \quad (18)$$

$$Z_{L_{loop}}^{\text{N,rd}}(s) = Z_S^{\text{NN}} + \frac{\det |Z_L^{\text{PN}}|}{Z_L^{\text{PP}}} = Z_S^{\text{NN}} + \frac{1}{Y_L^{\text{NN}}} \quad (19)$$

Expressions (18) and (19) is defined as the *reduced SISO model*, which is widely applied in previous research [8]. However, a frequency translation to phase domain is needed since this paper uses a dq frequency notation.

## C. Proof of Identical Marginal Stability Condition

This subsection will prove that the accurate SISO model is consistent with the MIMO model in terms of marginal stability condition. The marginal stability condition is defined as the case when the eigenvalue loci of a MIMO or SISO system cross the  $(-1, 0)$  point on the basis of GNC or NC.

For MIMO-based model, the marginal stability condition is:

$$\text{There is } s \text{ that eig}(Z_S^{\text{PN}} \cdot Y_L^{\text{PN}}) \text{ equals } -1 + 0 \cdot j \quad (20)$$

where  $Z_S^{\text{PN}}, Y_L^{\text{PN}}$  are given in (8) and (9). After some calculations, we have the equality as:

$$\det Z_S^{\text{PN}} + \det Z_L^{\text{PN}} + Z_S^{\text{PP}} Z_L^{\text{NN}} + Z_S^{\text{NN}} Z_L^{\text{PP}} - Z_L^{\text{NP}} Z_S^{\text{PN}} - Z_L^{\text{PN}} Z_S^{\text{NP}} = 0 \quad (21)$$

For SISO-based model, the marginal stability condition is:

$$\text{There is } s \text{ that eig}(Z_S^{\text{P}}/Z_L^{\text{P}}) \text{ equals } -1 + 0 \cdot j \quad (22)$$

where  $Z_S^{\text{P}}, Z_L^{\text{P}}$  are given in (15) and (16).

(22) is equivalent to  $\det |Z_{L_{loop}}^P| = 0 \rightarrow Z_{L_{loop}}^P = 0$ , thus the equality given by (13) is:

$$(Z_S^{\text{NN}} + Z_L^{\text{NN}})(Z_S^{\text{PP}} + Z_L^{\text{PP}}) - (Z_L^{\text{NP}} + Z_S^{\text{NP}})(Z_L^{\text{PN}} + Z_S^{\text{PN}}) = 0 \quad (23)$$

Expanding (23), then substitute  $\det Z_S^{\text{PN}} = Z_S^{\text{PP}} Z_S^{\text{NN}} - Z_S^{\text{NP}} Z_S^{\text{PN}}$  and  $\det Z_L^{\text{PN}} = Z_L^{\text{PP}} Z_L^{\text{NN}} - Z_L^{\text{PN}} Z_L^{\text{NP}}$  into (23) can prove that (21) equals (23), i.e., the accurate SISO model has the same marginal stability condition as the MIMO model. Therefore it can be used with accuracy in stability analysis. Furthermore, any modifications on SISO model will lead to a marginal stability condition different from (23) e.g., the reduced SISO model. Note that the same proof applies to the negative sequence.

## D. Comparison of SISO Models with Measurements

The accurate SISO model as in (13) and (14), and the reduced SISO model as in (18) and (19), will be compared under conditions of a) dq symmetric and b) dq asymmetric grid.

Impedance measurements conducted in PSCAD/EMTDC with the system in Fig. 1 (see Appendix A for detailed



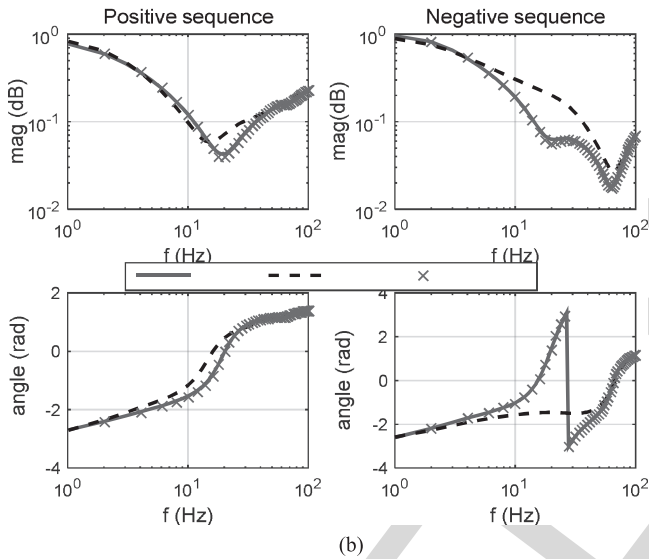
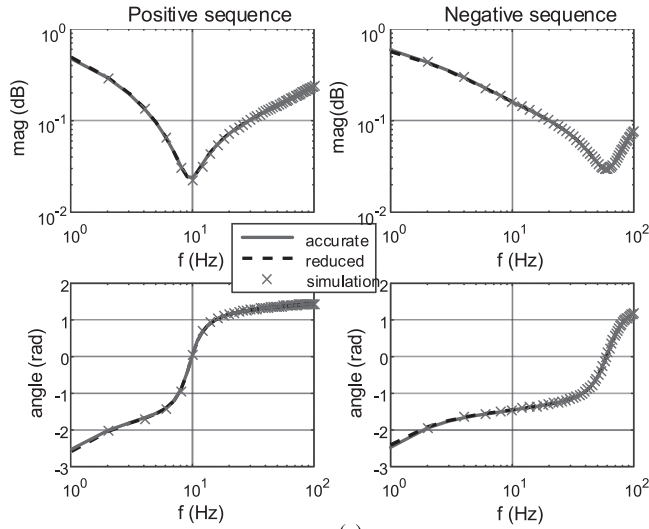


Fig. 5. Loop impedance comparison under dq symmetric grid. (a) SCR = 4, CC = 200 Hz, PLL = 5 Hz, current is 0.5 p.u. (flow out). (b) SCR = 4, CC = 200 Hz, PLL = 200 Hz, current is 0.5 p.u. (flow out).

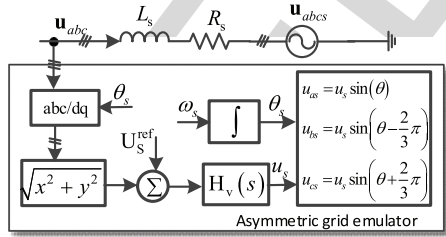


Fig. 6. Control scheme for asymmetric grid emulation.

284 system parameters). The multi-run module in PSCAD is used.  
 285 At each run, a single-tone harmonic voltage is injected into the  
 286 grid. The frequency is varied from 0 Hz to 100 Hz with an increment  
 287 of 2 Hz. The sampling frequency and sampling window  
 288 used for Fourier analysis are 1 kHz and 0.5 s respectively. All  
 289 data and figures are post-processed in MATLAB.

290 1) dq Symmetric Grid Cases: As shown in Fig. 5(a), both  
 291 accurate and reduced SISO models achieved a good match with

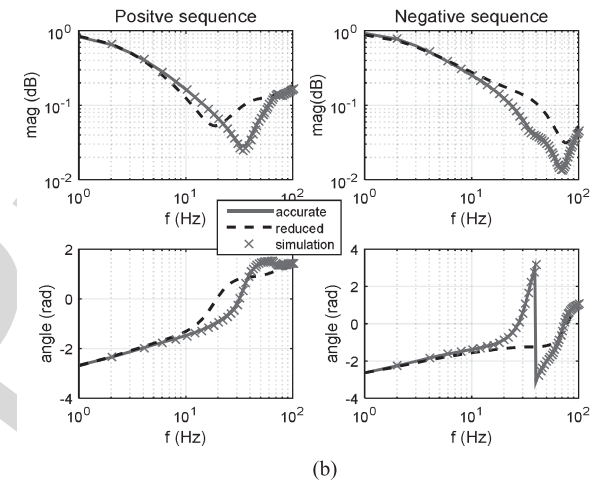
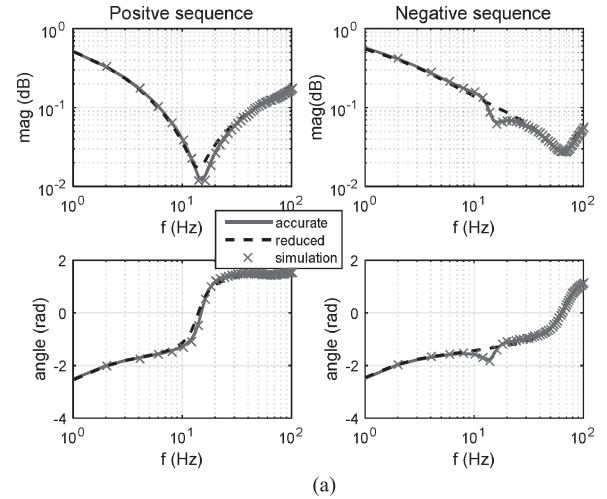


Fig. 7. Loop impedance comparison under dq asymmetric grid. (a) SCR = 4, CC = 200 Hz, PLL = 5 Hz, current is 0.5 p.u. (flow out) (Note that SCR here is only used for calculating grid passive impedance). (b) SCR = 4, CC = 200 Hz, PLL = 300 Hz, current is 0.5 p.u. (flow out) (Note that SCR here is only used for calculating grid impedance).

the measured impedances under a slow PLL configuration. However, if PLL bandwidth is increased to a relatively large value, the shapes of the reduced model would differ from the measurements, particularly for the negative sequence impedances, as shown in Fig. 5(b). By contrast, the accurate SISO model tracks the measured impedances accurately in Fig. 5(b). It proves that the accurate SISO model is superior to the reduced SISO model in capturing the details of impedance characteristics.

2) dq Asymmetric Grid Cases: In this paragraph, an actively controlled grid is introduced to emulate the asymmetric behavior in source subsystem.

**The control scheme is shown as below:**

In Fig. 6,  $\omega_s = 2\pi \cdot 50$  is constant,  $U_s^{\text{ref}}$  is the voltage amplitude set point of the active grid.  $H_v(s) = k_p^v + \frac{k_v^v}{s}$  is the voltage regulator. The sequence impedance of the actively controlled grid is asymmetric and can be found in Appendix. B ((A.1) and (A.2)).

Comparing Fig. 7(a) with Fig. 6(a) we can identify that, the good accuracy of reduced SISO model under symmetric grid as

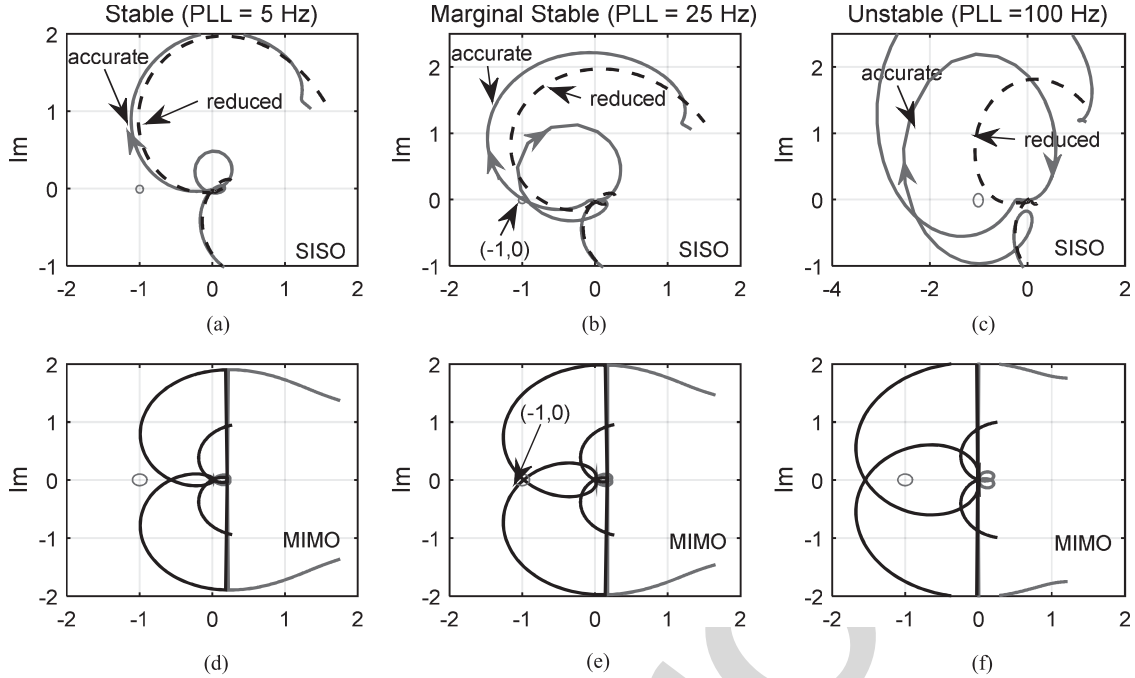


Fig. 8. Numerical stability comparisons with an asymmetric grid (SCR = 4, CC = 200 Hz, current is 0.5 p.u., dash line denotes locus of reduced SISO model, solid blue line denotes locus of accurate SISO model).

311 well as slow PLL configuration is violated if dq asymmetric  
 312 grid is presented. The inaccuracy of reduced SISO model can  
 313 be identified clearly in Fig. 7(b) as well, where a fast PLL is  
 314 adopted. On the contrary, the accurate SISO model still presents  
 315 good accuracy in all conditions.

#### 316 IV. SMALL-SIGNAL STABILITY ANALYSIS

317 This section will further analyze the validity of the proposed  
 318 SISO models in terms of small-signal stability, particularly for  
 319 the marginal stability condition in Section III-C. By acquiring  
 320 the advantages of SISO properties, the proposed model can be  
 321 used in combination with classic Nyquist criterion (NC) [23].

##### 322 A. Numerical Stability Analysis

323 Three model and criterion combinations are considered:

- 324 1) Reduced SISO with NC. (For comparison)
- 325 2) Accurate SISO with NC. (For comparison)
- 326 3) MIMO model with GNC. (For Reference).

327 In a, the eigenvalue loci is obtained straightforward as  
 328  $\lambda_P(s) = \mathbf{Z}_S^{PP} \cdot \mathbf{Y}_L^{PP}$  and  $\lambda_N(s) = \mathbf{Z}_S^{nn} \cdot \mathbf{Y}_L^{PP}$  in accordance with  
 329 (18) and (19).

330 In b, since the SISO loop impedance in (13) can be de-  
 331 composed into source and load subsystems as (15) and (16).  
 332 Therefore, the eigenvalue loci of minor loop gains are  $\lambda_P(s) =$   
 333  $\mathbf{Z}_S^P / \mathbf{Z}_L^P$  and  $\lambda_N(s) = \mathbf{Z}_S^n / \mathbf{Z}_L^P$ , where  $\mathbf{Z}_S^P, \mathbf{Z}_L^P, \mathbf{Z}_S^n, \mathbf{Z}_L^P$  are given  
 334 by (15)–(17).

335 In c, the eigenvalue loci can be calculated from  $\det$   
 336  $|\lambda \cdot \mathbf{I} - \mathbf{Z}_S^{PN} \mathbf{Y}_L^{PN}(s)| = 0$ , where  $\lambda_1(s), \lambda_2(s)$  are the two solu-  
 337 tions. The abovementioned eigenvalue loci are complex transfer  
 338 functions; thus, the locus for negative frequencies is not the

339 conjugation of the locus of positive frequencies [16]. How-  
 340 ever, the eigenvalue loci of SISO systems have the property  
 341  $(\lambda_N(j\omega))^* = \bar{\lambda}_N(-j\omega) = \lambda_P(-j\omega)$ . Hence, the negative fre-  
 342 quency plots can be obtained by conjugating the negative  
 343 sequence locus.

344 Fig. 8 illustrates the stability comparisons of three model and  
 345 criterion combinations under a dq asymmetric grid condition.  
 346 By varying PLL bandwidth in three steps from slow to fast, the  
 347 system is stable, marginal stable and unstable respectively. The  
 348 accurate SISO model with NC has the same stability conclusion  
 349 as the MIMO model with GNC. Particularly, the eigenvalue loci  
 350 of accurate SISO model and MIMO model cross the  $(-1, 0j)$   
 351 point simultaneously, indicating that the proof of marginal sta-  
 352 bility condition in Section III-C is correct. On the other hand,  
 353 the reduced SISO model fails to give the correct marginal sta-  
 354 bility condition, as well as the stability conclusion, identified in  
 355 Figs. 8(b) and (c) respectively.

356 Therefore, it is not safe to use the reduced SISO model if the  
 357 converter and grid is highly dq asymmetric. On the contrary,  
 358 the accurate SISO model is effective for stability analysis in this  
 359 respect.

360 The marginal stability can also be analyzed physically by find-  
 361 ing the damping characteristic at resonances of loop impedance,  
 362 e.g., by passivity analysis in [24]. The following time domain  
 363 study will provide more physical insights into the oscillatory  
 364 behavior lies in the grid-tied VSC system.

##### 365 B. Simulation Study

366 The physical interpretation of marginally stable condition is  
 367 that the loop impedance has approximately zero damping at a  
 368 resonance frequency. By plotting the real and imaginary parts

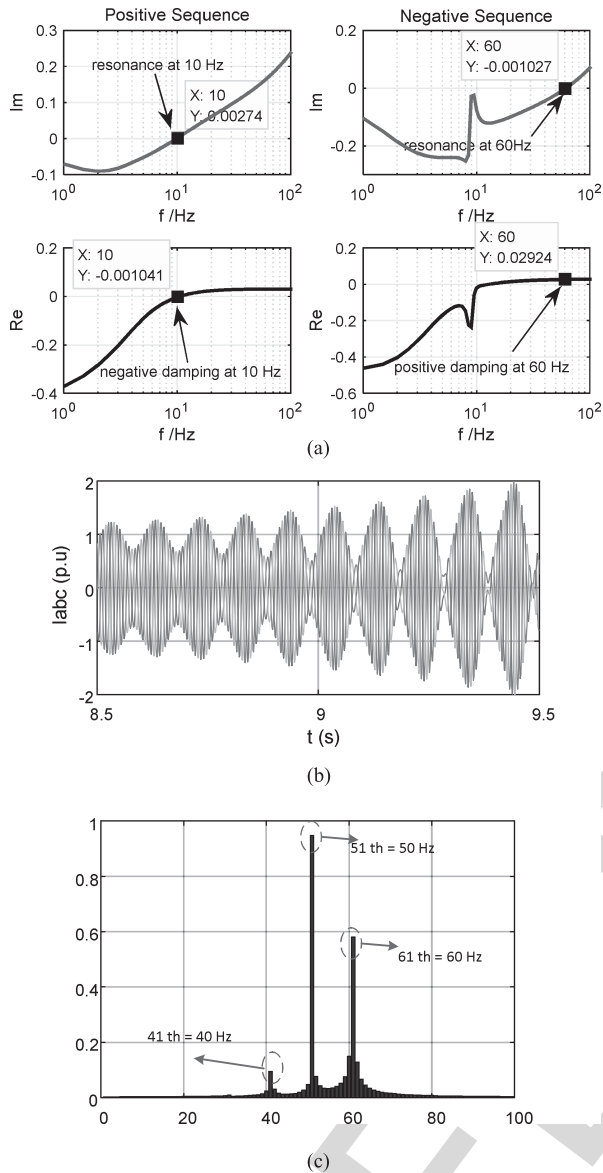


Fig. 9. Marginally stable analysis (CC = 200 Hz SCR = 4, VSC current is 1 p.u.). (a) Positive and negative sequence loop impedance plots. (b) Time domain simulation. (Before 2 seconds, the PLL bandwidth is 5 Hz to achieve a stable operational point. Afterwards, the PLL bandwidth is set to 20 Hz. Oscillation is observable after several seconds.) (c) Fourier analysis of phase current. (Sampling rate is 1 kHz. Sampling window is 1 second.)

of loop impedance, the resonances can be found at frequencies where the imaginary part cross zero axis, meanwhile damping at these resonances can be determined according to the sign of real parts.

As shown in Fig. 9(a), the positive sequence loop impedance has a resonance at 10 Hz, while the negative sequence loop impedance has a resonance at 60 Hz, this findings is consistent with the analytical calculation of resonant points in [22]. Furthermore, the damping at 10 Hz resonance is negative with small value, indicating a marginally unstable condition, on the contrary a positive damping characteristic is presented at 60 Hz, indicating a stable resonance. It is again emphasized that the resonance frequencies are referred to dq frame in the above analysis.

Time domain simulations in PSCAD/EMTDC also draw similar conclusions in terms of stability. The VSC output currents gradually become unstable during a long simulation time in Fig. 9(b), this is due to the fact that negative damping at 10 Hz is small.

Furthermore, by performing a Fourier analysis on the phase current, we can identify that two additional frequencies except the fundamental at 40 Hz and 60 Hz appears, the *mirror frequency coupling effect* is originated from oscillations in dq frame at 10 Hz, which again proves the correctness of above analysis. Additionally, the oscillatory behavior shown in Fig. 9(b) is also similar to the field measurements of grid-tied photovoltaic inverter systems in [25].

## V. CONCLUSION

This paper developed a generalized method for converting dq impedance model of grid-tied VSC system into its SISO sequence domain equivalents. The converting process includes two steps: firstly converts dq impedance into its MIMO sequence domain equivalent, then converts the MIMO sequence domain equivalent into its SISO equivalent by means of closed-loop analysis method proposed in this paper. The decoupled SISO model allows the classic Nyquist Criterion to be used for stability analysis.

Two types of SISO model were given, the accurate one is directly from the consequence of conversion, and the reduced one is derived with a strong grid condition approximation. Numerical and time domain analysis shown that the reduced SISO model gives the wrong stability conclusions in cases where the system is highly dq asymmetric. On the contrary, the accurate SISO model presents a good consistence with MIMO model in terms of stability conclusions, particularly for the marginally stable condition.

The proposed method is general for any MIMO LTI systems. Therefore it is applicable to grid-tied VSC systems where a power controller or DC voltage controller is adopted. Only the marginal stability condition is proven to be identical in this work. Performance on gain and phase margin should be carefully evaluated in future works.

## APPENDIX

### A. Circuit Parameters Used in Stability Analysis and Simulations

TABLE A1  
CIRCUIT PARAMETERS OF THE GRID-TIED VSC SYSTEM

NAME	VALUES	NAME	VALUES
Nominal rating	2 MVA	Filter inductance	0.1 p.u.
Nominal voltage	0.69 kV	Grid inductance (SCR = 4)	1/SCR = 0.25 p.u.
Dc voltage	1.1 kV	Current controller (CC = 200 Hz)	$k_p^c = 0.03, k_i^c = 6.1$
Switching frequency	2.4 kHz	PLL controller (PLL = 20 Hz)	$k_p^{pll} = 71, k_i^{pll} = 1421$
		asymmetric grid controller	$k_p^v = 1, k_i^v = 100$



## 424 B. Modeling of Actively Controlled Grid

425 The dq domain grid model with control scheme in Fig. 6 is:

$$\mathbf{Z}_{\text{grid}}^{\text{dq}}(s) = \begin{bmatrix} 1 + \cos \delta_0 H_V(s) & 0 \\ -\sin \delta_0 H_V(s) & 1 \end{bmatrix} \begin{bmatrix} sL_s + R_s & -\omega_s L_s \\ \omega_s L_s & sL_s + R_s \end{bmatrix} \quad (\text{A.1})$$

426 where  $\delta_0$  is the steady voltage angle difference between PCC and  
427 grid. Clearly, the dq impedance of actively controlled grid is  
428 not symmetric. Using the decomposition method in Section II-B  
429 gives a coupled sequence impedance:

$$\mathbf{Z}_{\text{grid}}^{\text{PN}}(s) = \mathbf{A} \mathbf{Z}_{\text{grid}}^{\text{dq}}(s) \mathbf{A}^{-1} \quad (\text{A.2})$$

## 430 C. dq Symmetric and Asymmetric

431 For a dq impedance matrix  $\begin{bmatrix} Z^{\text{dd}}(s) & Z^{\text{dq}}(s) \\ Z^{\text{qd}}(s) & Z^{\text{qq}}(s) \end{bmatrix}$ , it is said to be  
432 dq symmetric if  $Z^{\text{dd}}(s) = Z^{\text{qq}}(s)$  and  $Z^{\text{dq}}(s) = -Z^{\text{qd}}(s)$ , and  
433 if the condition not satisfied, the system is referred to dq asym-  
434 metric. For a dq symmetric system, its sequence equivalent  
435 can be obtained by linear transformation using the methods in  
436 Section II. As a result, the sequence impedance is decoupled.  
437 Otherwise, the sequence impedance is coupled.

## 438 REFERENCES

- 439 [1] R. Teodorescu, M. Liserre, and P. Rodriguez, "Introduction," in *Grid*  
440 *Converters for Photovoltaic and Wind Power Systems*. Chichester, U.K.:  
441 Wiley, 2011, pp. 1–4.  
442 [2] N. Flourentzou, V. G. Agelidis, and G. D. Demetriades, "VSC-Based  
443 HVDC power transmission systems: An overview," *IEEE Trans. Power*  
444 *Electron*, vol. 24, no. 3, pp. 592–602, Mar. 2009.  
445 [3] D. Dong, B. Wen, D. Boroyevich, P. Mattavelli, and Y. Xue, "Analysis of  
446 phase-locked loop low-frequency stability in three-phase grid-connected  
447 power converters considering impedance interactions," *IEEE Trans. Ind.*  
448 *Electron.*, vol. 62, no. 1, pp. 310–321, Jan. 2015.  
449 [4] L. P. Kunjumammed, B. C. Pal, C. Oates, and K. J. Dyke, "Electrical  
450 oscillations in wind farm systems: Analysis and insight based on detailed  
451 modeling," *IEEE Trans. Sustain. Energy*, vol. 7, no. 1, pp. 51–62, Jan.  
452 2015.  
453 [5] D. Yang, X. Ruan, and H. Wu, "Impedance shaping of the grid-connected  
454 inverter with LCL filter to improve its adaptability to the weak grid condi-  
455 tion," *IEEE Trans. Power Electron*, vol. 29, no. 11, pp. 5795–5805, Nov.  
456 2014.  
457 [6] L. Harnefors, M. Bongiorno, and S. Lundberg, "Input-admittance calcu-  
458 lation and shaping for controlled voltage-source converters," *IEEE Trans.*  
459 *Ind. Electron.*, vol. 54, no. 6, pp. 3323–3334, Dec. 2007.  
460 [7] M. Belkhat, "Stability criteria for AC power systems with regulated  
461 loads," Ph.D. dissertation, Purdue University, West Lafayette, IN, USA,  
462 1997.  
463 [8] M. Cespedes and J. Sun, "Impedance modeling and analysis of grid-  
464 connected voltage-source converters," *IEEE Trans. Power Electron.*,  
465 vol. 29, no. 3, pp. 1254–1261, Mar. 2014.  
466 [9] B. Wen, D. Boroyevich, R. Burgos, P. Mattavelli, and Z. Shen, "Small-  
467 signal stability analysis of three-phase AC systems in the presence of  
468 constant power loads based on measured d-q, frame impedances," *IEEE*  
469 *Trans. Power Electron.*, vol. 30, no. 10, pp. 5952–5963, Oct. 2015.  
470 [10] S. Shah and L. Parsa, "On impedance modeling of single-phase voltage  
471 source converters," in *Proc. IEEE Energy Convers. Congr. Expo.*, 2016,  
472 pp. 1–8.  
473 [11] J. Lyu, X. Cai, and M. Molinas, "Impedance modeling of modular  
474 multilevel converters," in *Proc. Annu. Conf. IEEE Ind. Electron. Soc.*,  
475 Yokohama, Japan, 2015, pp. 180–185.

- [12] J. Sun, "Small-signal methods for AC distributed power systems—A review," in *Proc. IEEE Electr. Ship Technol. Symp.*, 2009, pp. 44–52. 476  
477  
[13] E. Möllerstedt, "Dynamic analysis of harmonics in electrical systems," 478  
Ph.D. dissertation, Dept. Automat. Control, Lund University, Lund, 479  
Sweden, 2000. 480  
[14] M. K. Bakhshizadeh *et al.*, "Couplings in phase domain impedance mod- 481  
eling of grid-connected converters," *IEEE Trans. Power Electron*, vol. 31, 482  
no. 10, pp. 6792–6796, Oct. 2016. 483  
[15] S. Shah and L. Parsa, "Sequence domain transfer matrix model of three- 484  
phase voltage source converters," in *Proc. IEEE Power Energy Soc. Gener- 485  
al Meet.*, 2016, pp. 1–5. 486  
[16] L. Harnefors, "Modeling of three-phase dynamic systems using com- 487  
plex transfer functions and transfer matrices," *IEEE Trans. Ind. Electron*, 488  
vol. 54, no. 4, pp. 2239–2248, Aug. 2007. 489  
[17] A. Rygg, M. Molinas, C. Zhang, and X. Cai, "A modified sequence domain 490  
impedance definition and its equivalence to the dq-domain impedance 491  
definition for the stability analysis of ac power electronic systems," *IEEE 492  
J. Emerg. Sel. Topics Power Electron.*, vol. 4, no. 4, pp. 1382–1396, Dec. 493  
2016. 494  
[18] G. C. Paap, "Symmetrical components in the time domain and their appli- 495  
cation to power network calculations," *IEEE Trans. Power Syst*, vol. 15, 496  
no. 2, pp. 522–528, May 2000. 497  
[19] X. Wang, L. Harnefors, F. Blaabjerg, and P.C. Loh, "A unified impedance 498  
model of voltage-source converters with phase-locked loop effect," in 499  
*Proc. IEEE Energy Convers. Congr. Expo.*, 2016, pp. 1–8. 500  
[20] J. Kwon, X. Wang, F. Blaabjerg, C. L. Bak, V. S. Sularea, and C. Busca, 501  
"Harmonic interaction analysis in grid-connected converter using Har- 502  
monic State Space (HSS) modeling," *IEEE Trans. Power Electron.*, vol. 32, 503  
no. 9, pp. 6823–6835, Sep. 2016. 504  
[21] C. Desoer and Y.T. Wang, "On the generalized nyquist stability crite- 505  
rion," *IEEE Trans. Autom. Control*, vol. 25, no. 2, pp. 187–196, Apr. 506  
1980. 507  
[22] C. Zhang, X. Cai, Z. Li, A. Rygg, and M. Molinas, "Properties and phys- 508  
ical interpretation of the dynamic interactions between voltage source 509  
converters and grid: Electrical oscillation and its stability control," *IET 510  
Power Electron.*, vol. 10, no. 8, pp. 894–902, Jun. 2017. 511  
[23] J. Sun, "Impedance-based stability criterion for grid-connected invert- 512  
ers," *IEEE Trans. Power Electron*, vol. 26, no. 11, pp. 3075–3078, Nov. 513  
2011. 514  
[24] L. Harnefors, X. Wang, A. G. Yepes, and F. Blaabjerg, "Passivity-based 515  
stability assessment of grid-connected VSCs—An overview," *IEEE J. 516  
Emerg. Sel. Topics Power Electron.*, vol. 4, no. 1, pp. 116–125 Mar. 517  
2016. 518  
[25] C. Li, "Unstable operation of photovoltaic inverter from field experiences," 519  
*IEEE Trans. Power Del.*, to be published. 520



**Chen Zhang** received the B.Eng. degree in electrical engineering from China University of Mining and Technology, Xuzhou, China, in 2011. He is currently working toward the Ph.D. degree in electrical engineering with Shanghai Jiao Tong University, Shanghai, China. He was a Ph.D. Visiting Scholar in the Department of Engineering Cybernetics, Norwegian University of Science and Technology, Trondheim, Norway, in 2015. His current research interests include modeling and stability analysis of VSC-based energy conversion systems, where the aim is to reveal the fundamental dynamics and stability mechanisms of renewable energies with VSCs as the grid interface.

535  
536  
537  
538  
539  
540  
541  
542  
543  
544  
545  
546  
547  
548  
549  
550  
551



**Xu Cai** received the B.Eng. degree from Southeast University, Nanjing, China, in 1983, and the M.Sc. and Ph.D. degrees from China University of Mining and Technology, Xuzhou, China, in 1988 and 2000, respectively. He was in the Department of Electrical Engineering, China University of Mining and Technology, as an Associate Professor, from 1989 to 2001. He was the Vice Director of the State Energy Smart Grid R&D Center, Shanghai, China, from 2010 to 2013. He has been with Shanghai Jiao Tong University, Shanghai, as a Professor, since 2002, where he

has also been the Director of the Wind Power Research Center, since 2008. His current research interests include power electronics and renewable energy exploitation and utilization, including wind power converters, wind turbine control system, large power battery storage systems, clustering of wind farms and its control system, and grid integration.

552  
553  
554  
555  
556  
557  
558  
559  
560  
561  
562  
563



**Atle Rygg** received the M.Sc. degree in electrical engineering from Norwegian University of Science and Technology (NTNU), Trondheim, Norway, in 2011. He is currently working toward the Ph.D. degree in Department of Engineering Cybernetics at NTNU. From 2011 to 2015, he was a Research Scientist at SINTEF Energy Research in the field of power electronics. His topic or research interests include impedance based stability analysis of power electronic systems, where the aim is to contribute to the fundamental understanding in this family of methods.



**Marta Molinas** (M'94) received the Diploma degree in electromechanical engineering from the National University of Asuncion, Asuncion, Paraguay, in 1992, the Master of Engineering degree from Ryukyu University, Nishihara, Japan, in 1997, and the Doctor of Engineering degree from Tokyo Institute of Technology, Tokyo, Japan, in 2000. She was a Guest Researcher with the University of Padova, Padova, Italy, during 1998. From 2004 to 2007, she was a Postdoctoral Researcher with the Norwegian University of Science and Technology (NTNU) and

from 2008 to 2014 she has been Professor in the Department of Electric Power Engineering at the same university. She is currently a Professor in the Department of Engineering Cybernetics, NTNU. Her research interests include stability of power electronics systems, harmonics, instantaneous frequency, and nonstationary signals from the human and the machine. She is an Associate Editor for the IEEE JOURNAL OF EMERGING AND SELECTED TOPIC IN POWER ELECTRONICS, the IEEE TRANSACTIONS ON POWER ELECTRONICS and an Editor of the IEEE TRANSACTIONS ON ENERGY CONVERSION. She has been an AdCom Member of the IEEE Power Electronics Society from 2009 to 2011.

564  
565  
566  
567  
568  
569  
570  
571  
572  
573  
574  
575  
576  
577  
578  
579  
580  
581  
582  
583  
584

IEEE PROCEEDINGS

586 Q1. Author: Please provide the department name in Ref. [7].

587 Q2. Author: Please update Ref. [25].

Dear Editor,

Thank you for your review.

Regarding Q1, the reference is updated as bellow :

[7] Belkhat M, "Stability criteria for AC power systems with regulated loads," Ph.D. dissertation, Dept. Electrical Engineering, Purdue University, West Lafayette, IN, USA, 1997.

Regarding Q2, the reference is updated as bellow:

[25] C. Li, "Unstable Operation of Photovoltaic Inverter from Field Experiences," IEEE Trans. Power Del, doi: 10.1109/TPWRD.2017.2656020.

Besides, i add two comments in the context, please refer to line 191 and line 303 respectively.

If anything is inappropriate please let me know, thank you !

Sincerely,

Chen Zhang